© 2016. Published by The Company of Biologists Ltd | Journal of Cell Science (2016) 129, 2817-2828 doi:10.1242/jcs.184382

RESEARCH ARTICLE

Organelle size control – increasing vacuole content activates SNAREs to augment organelle volume through homotypic fusion

Yann Desfougères[1], Heinz Neumann[2] and Andreas Mayer[1,*]

ABSTRACT

Cells control the size of their compartments relative to cell volume, but there is also size control within each organelle. Yeast vacuoles neither burst nor do they collapse into a ruffled morphology, indicating that the volume of the organellar envelope is adjusted to the amount of content. It is poorly understood how this adjustment is achieved. We show that the accumulating content of yeast vacuoles activates fusion of other vacuoles, thus increasing the volume-to-surface ratio. Synthesis of the dominant compound stored inside vacuoles, polyphosphate, stimulates binding of the chaperone Sec18/NSF to vacuolar SNAREs, which activates them and triggers fusion. SNAREs can only be activated by lumenal, not cytosolic, polyphosphate (polyP). Control of lumenal polyP over SNARE activation in the cytosol requires the cytosolic cyclin-dependent kinase Pho80–Pho85 and the R-SNARE Nyv1. These results suggest that cells can adapt the volume of vacuoles to their content through feedback from the vacuole lumen to the SNAREs on the cytosolic surface of the organelle.

KEY WORDS: Membrane fusion, Organelle size, Polyphosphate, SNAREs, Vacuole, Lysosome

INTRODUCTION

Maintaining membrane tension of an organelle while avoiding its lysis requires correspondence between the amount of content and the volume provided by the boundary membrane. Maintaining this correspondence is likely to be functionally important because the activity of many membrane proteins, such as transporters and channels, can depend on the tension of the membrane they reside in (Hamill and Martinac, 2001; Sukharev and Sachs, 2012), and the complexes and activities of soluble proteins in the organelle lumen are greatly influenced by macromolecular crowding (Zhou et al., 2008). Furthermore, specific interactions of macromolecules inside the organelle are affected by their concentration. Adjustment of the surface-to-volume ratio of an organelle can assure optimal membrane tension and appropriate concentrations for the soluble content of the organelle. Fusion and fission of the multiple copies of a compartment provide a rapid and efficient way of achieving this because they are independent of new membrane synthesis and readily reversible. These mechanisms are also expected to serve in the adjustment of organelle volume to correlate with cell size, a ratio that is kept surprisingly constant under steady-state growth conditions but which can change considerably as the growth conditions of a cell change (Marshall, 2012). However, we can expect that other processes also contribute to the adjustment, such as the net influx and efflux of membrane, or modifications of organelle shape. Changes in organellar size and/or organellar surface-to-volume ratio have been observed – e.g. for the Golgi, vacuoles, mitochondria and endosomes (Banta et al., 1988; Bevis et al., 2002; Bhave et al., 2014; Chan and Marshall, 2014; Gaynor et al., 1998; Seeley et al., 2002).

The size of several organelles or protein assemblies has been reported to be actively regulated (Katsura, 1987; Levy and Heald, 2010; Ludington et al., 2012), but it remains poorly understood how size control is achieved at the molecular level. Under constant growth conditions, the size of membrane-enclosed organelles scales with cell size (Chan and Marshall, 2012). Upon changes in growth conditions, the macromolecular content and the volume occupied by an organelle type can be altered both in absolute terms and relative to the cell surface. Because organelles remain intact during such changes and do not burst, cells might be capable of controlling the volume of the organellar boundary membrane relative to organelle content. One way in which this can be achieved are shape changes, because all deviations from a spherical shape will decrease the volume-to-surface ratio. Non-spherical shapes of membranes can be dictated by proteins or by changes in lipid distribution (Derganc et al., 2013; Frolov et al., 2011; Heald and Cohen-Fix, 2014; Rafelski and Marshall, 2008). Manipulation of the balance of membrane influx and efflux pathways can also increase or decrease the volume of the organellar envelope. For example, a mutation reducing vesicular traffic from vacuoles to endosomes or the Golgi (*atg18*Δ) increases the volume of yeast vacuoles, whereas reductions in membrane influx (*apl5*Δ) decrease it (Chan and Marshall, 2014; Dove et al., 2004; Efe et al., 2007; Tamura et al., 2013; Zieger and Mayer, 2012). A third possibility is the fusion or fission of the organelle. Fusion of several organelle copies will increase the volume-to-surface ratio without a need for new membrane synthesis, fission will do the reverse. So far, however, these mechanisms have not been implicated in adjusting the volume of the organellar envelope to the amount of content to be enclosed. We have begun to study this question with the lysosome-like vacuoles of yeast cells.

Lysosomes and vacuoles are dynamic organelles (Settembre et al., 2012; Weisman, 2003). During starvation and autophagy, lysosomal hydrolases are induced to a large extent. The resulting augmentation of macromolecular content is accompanied by a volume increase of the lysosomal boundary membrane (Yu et al., 2010). During this volume increase, as well as during its reversal, the boundary membrane neither explodes nor does it collapse into a ruffled morphology. It appears to retain a well-inflated appearance, which suggests that the volume-to-surface ratio of the organelle envelope might be controlled. This can help to maintain

[1]Département de Biochimie, Université de Lausanne, Chemin des Boveresses 155, Epalinges 1066, Switzerland. [2]GZMB, Institut für Molekulare Strukturbiologie, Georg-August-Universität Göttingen, Justus-von-Liebig-Weg 11, 37077 Göttingen, Germany.

*Author for correspondence (andreas.mayer@unil.ch)

A.M., 0000-0001-6131-313X

Received 4 December 2015; Accepted 26 May 2016

Journal of Cell Science (2016) 129, 2817-2828 doi:10.1242/jcs.184382

the membrane tension and the concentration of lumenal macromolecules that are crucial for organelle function (Ellis, 2001; García-Pérez et al., 1999; Heald and Cohen-Fix, 2014; Upadhyaya and Sheetz, 2004).

We explore the hypothesis that the volume of the boundary membrane of vacuoles adapts to the amount of content to be enclosed through use of membrane fusion or fission. Vacuoles are good objects to study this question. Their size and copy number are influenced by an equilibrium of membrane fusion and fission (Baars et al., 2007; Efe et al., 2007; Zieger and Mayer, 2012) and by environmental changes (Peters et al., 2004; Weisman, 2003). A crucial advantage is that vacuole content is dominated by only few compounds, polyphosphate (polyP) and the basic amino acids that associate with it (Saito et al., 2005). PolyP is a polymer of up to hundreds of inorganic phosphate units linked by phospho-anhydride bonds. It is a storage form of phosphate, a compound that is often growth-limiting for plants, fungi and bacteria. PolyP occurs also in mammalian lysosomes, but here its function is unknown (Pisoni and Lindley, 1992). Yeast synthesizes polyP through the vacuolar transporter chaperone (VTC) complex, which is located in the vacuolar membrane and comprises three subunits (Vtc1, Vtc3 and Vtc4) (Hothorn et al., 2009). Vacuolar polyP can constitute up to 15% of the dry weight of a yeast cell. Because the vacuole occupies less than a third of the volume of a yeast cell but contains virtually all cellular polyP, polyP can constitute >50% of the vacuolar dry weight. Thus, manipulating the synthesis of polyP grossly changes vacuole content.

Vacuoles respond to increases in their osmotic pressure through fusion, and *in vitro* experiments have identified the stimulation of Rab-GTPase-mediated vacuole docking as one of the effects responsible for this change (Brett and Merz, 2008). Our earlier work has identified the VTC complex as a factor that is necessary for vacuole fusion and for priming of SNARE proteins (Müller et al., 2002, 2003). Given that the VTC complex interacts with parts of the vacuolar fusion machinery, such as the R-SNARE Nyv1 and the V_0 sector of the V-ATPase, we had interpreted the effects of VTC deletion on fusion as a consequence of the loss of these interactions. Because VTC has since been identified as the major polyP polymerase of yeast (Hothorn et al., 2009), we have reconsidered the role of VTC in vacuole fusion and have now tested whether it could stimulate vacuole fusion by changing the abundance of vacuole content. We exploited the availability of structural information on the catalytic center of VTC and of methods to reliably measure synthesis and translocation of polyP by yeast vacuoles (Gerasimaite et al., 2014) in order to explore a possible link between the vacuolar fusion machinery and polyP accumulation in the vacuolar lumen.

RESULTS

Polyphosphate synthesis and accumulation is required for homotypic vacuole fusion

We asked whether the synthesis of polyP might trigger a corresponding increase in vacuolar storage space for this compound. Fusing the multiple vacuoles of a cell into a single organelle of larger volume could achieve this (Fig. 1A). We used the vital dye FM4-64 (Vida and Emr, 1995) to stain vacuoles in yeast cells that did not accumulate polyP because they contain inactive VTC complexes (Fig. 1B,C). When grown on synthetic Hartwell's complete medium, numerous small vacuoles were found in cells carrying the catalytically inactive vtc4^{R264A} as well as in the deletion mutants *vtc4*Δ and *vtc1*Δ. Wild-type cells showed mostly 1–2 large vacuoles. This is in contrast with our earlier observations that, similar to *nyv1*Δ cells, *vtc4*Δ cells cultured in yeast extract peptone dextrose (YPD) medium carry a single large vacuole (Müller et al., 2001) (Fig. S1). This difference could be explained by an osmotic imbalance, resulting from the composition of YPD medium, which contains four-times more of the amino acids Arg, Lys and His than Hartwell's complete medium. These three amino acids accumulate in vacuoles to very high concentrations, and this effect is much more pronounced on YPD than on synthetic medium (Kitamoto et al., 1988). In absence of polyP, which normally sequesters and osmotically inactivates these amino acids (Dürr et al., 1979), the excess of vacuolar amino acids might create an osmotic pressure that hinders the organelle from fragmenting in YPD-grown *vtc* mutants.

The tendency of *vtc1*Δ and *vtc4*Δ cells to show fragmented vacuoles is an indicator for reduced vacuolar fusion activity. We tested whether vacuolar polyP stimulates vacuole fusion by comparing the fusion activity of isolated vacuoles to their rate of polyP accumulation. Purified vacuoles fuse when incubated with ATP (Wickner, 2010). Under the same conditions, they also synthesise polyP efficiently, reaching up to 0.4 µg of polyP per µg of vacuolar protein within 20 min (Fig. 2A). Structure–function analyses of the VTC complex identified missense mutations and/or single residue substitutions that impair or stimulate polyP synthesis without affecting the structural integrity of the complex (Hothorn et al., 2009). These substitutions lie either in the catalytic domain of Vtc4, which is oriented towards the cytosol and converts ATP into polyP and ADP; in the cytosolic SPX domains, which are assumed to have regulatory function; or in the transmembrane domains of Vtc1, which are believed to translocate the polyP chain across the membrane (Gerasimaite et al., 2014; Hothorn et al., 2009; Wild et al., 2016). This set of mutations includes the catalytic domain substitution vtc4^{K200A}, which permits Vtc4 to hydrolyze ATP, but without producing polyP (Hothorn et al., 2009). Fusion activity of vacuoles from the respective mutants increased with the rate of polyP accumulation (Fig. 2B). Because the single amino acid substitutions in the Vtc proteins allow assembly of the VTC complex and its sorting to the vacuole (Hothorn et al., 2009; Wild et al., 2016), this result suggests that the vacuolar fusion machinery might be controlled by the accumulation of polyP inside the vacuoles independently of the physical presence of the VTC complex.

Cytosolic polyphosphate does not affect vacuole fusion

Next, we compared the effects of the lumenal fraction of polyP and of an artificially generated cytosolic pool of polyP on vacuole fusion. VTC has been proposed to act as an obligatorily coupled synthase and translocase (Gerasimaite et al., 2014). Its cytosolic domains synthesize polyP and feed it directly into the vacuolar lumen through the VTC transmembrane domains. Therefore, VTC produces lumenal polyP rather than freely diffusible cytosolic polyP (Saito et al., 2005). The luminal pool can be reduced by engineering the delivery of a polyphosphatase into the vacuolar lumen. In this way, the VTC complex remains unmodified and continues to synthesize polyP, but polyP accumulation in the lumen is nevertheless reduced. We used a fusion of the polyphosphatase Ppx1 with the pre-pro-sequence of the vacuolar carboxypeptidase Y (Prc1), which targets the fusion protein through the ER, Golgi and endosomes into the vacuolar lumen (Gerasimaite et al., 2014). This construct can only be used in strains deficient in vacuolar proteases, such as BJ3505, because it is degraded in protease-proficient vacuoles. Vacuolar Ppx1 converts polyP into inorganic phosphate and oligophosphates (Wurst and Kornberg, 1994). Inorganic phosphate can then be exported into the cytosol by Pho91 (Hürlimann et al., 2007). A GFP-tagged version of this construct

Journal of Cell Science

Journal of Cell Science (2016) 129, 2817-2828 doi:10.1242/jcs.184382

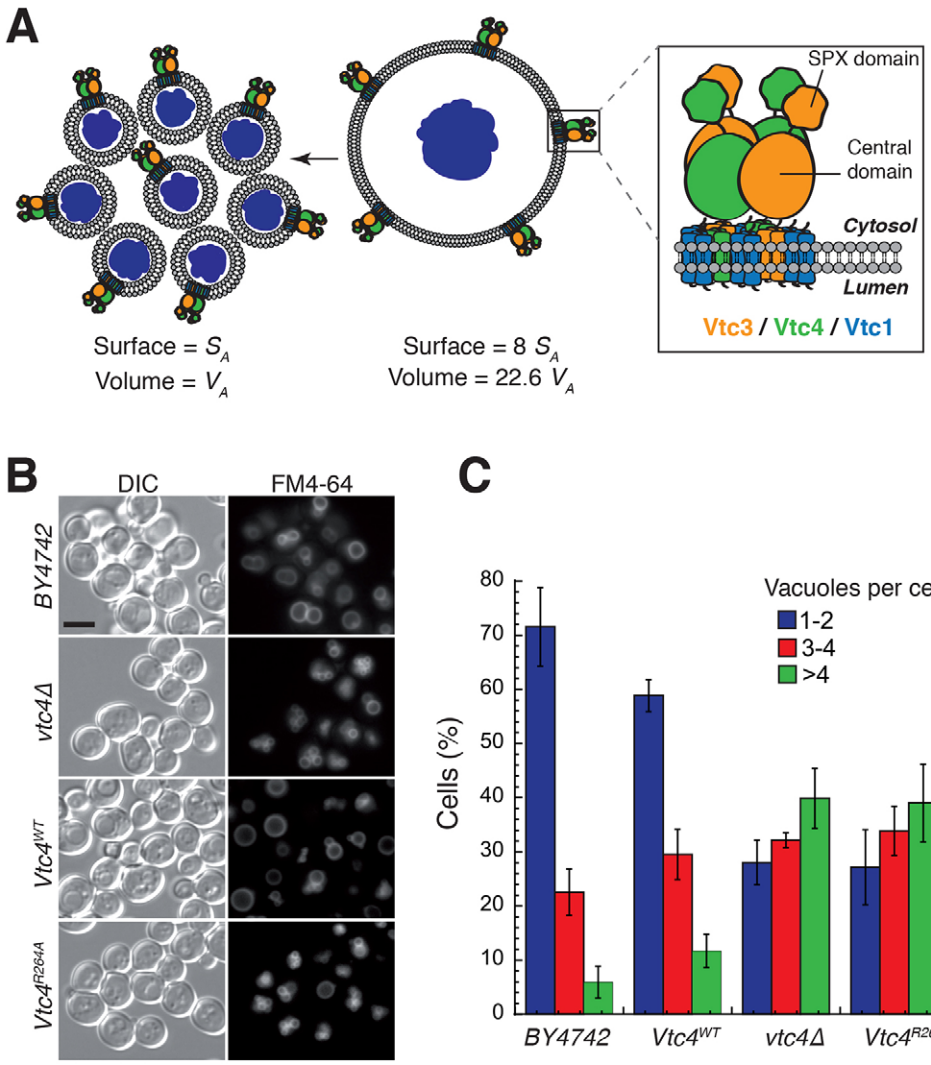

Fig. 1. Influence of polyP accumulation on vacuole morphology *in vivo*. (A) Schematic representation of the change in vacuole volume through fusion. Fusion of eight small vacuoles of equal size into a single vacuole increases the enclosed volume by >20-fold. (B) Vacuole morphology. Wild-type or the indicated *vtc* mutant strains were grown in Hartwell's complete medium, stained with 10 µM FM4-64 for 1 h, washed twice in Hartwell's complete medium and incubated in fresh Hartwell's complete medium for two hours at 30°C. The cells were analyzed with fluorescence microscopy. Scale bar: 5 µm. (C) The number of vacuoles per cell was counted for at least 250 cells per experiment (n=3). Data are mean±s.d. WT, wild type.

yielded strong GFP-staining of the vacuolar lumen, no staining in the cytosol and only very weak signals in the cell periphery and around nuclei, which we interpreted as being staining of the ER (Fig. 2C) (Gerasimaite et al., 2014). Whole-cell extracts showed no significant degradation of the fusion protein (Fig. S2), suggesting that the construct is correctly targeted to vacuoles. Vacuole-targeted Ppx1 reduced the *in vivo* polyP content of BJ3505 cells by 90%. It reduced the *in vitro* polyP accumulation of their vacuoles by 80% (Fig. 2D) and their fusion activity by 40% (Fig. 2E), suggesting that the lumenal pool of polyP influenced fusion activity. It should be noted that in this experiment, polyP accumulation could be reduced only in one of the fusion partners – i.e. in the protease-deficient BJ3505 vacuoles – whereas the construct could not be used in the other protease-competent fusion partner from DKY6281 cells, where it would be degraded. This can explain why fusion activity is less affected than polyP accumulation. Furthermore, the reduction in polyP might be overestimated because Ppx1 shows >100 times higher K_m values for short chains (<10 residues) than for long chains (>50 residues), and it cannot degrade short end-products, such as pyrophosphate (Wurst and Kornberg, 1994). Such short species might remain in the vacuoles of cells expressing vacuole-targeted Ppx1, but they do not induce the shift in DAPI fluorescence that is the basis for detection by our polyP assay (Omelon et al., 2016).

If the presence of polyP at the cytosolic side constitutes a signal for vacuolar fusion, the addition of polyP to the buffer should substitute for polyP synthesis by VTC. We isolated vacuoles from *vtc4*Δ and *vtc4*^{R264A} cells and incubated them in fusion reactions containing synthetic polyP of an average chain length of 60 and 300 phosphate residues (polyP-60 and polyP-300, respectively), which covers the range of chain lengths produced by the VTC complex (Hothorn et al., 2009; Lonetti et al., 2011) but which is not imported by the vacuoles (Gerasimaite et al., 2014). In tests over a wide range of different concentrations, polyP-60 and polyP-300 that had been added to the cytosolic side could not stimulate fusion (Fig. 2F). Taken together, these observations suggest that only lumenal polyP promotes fusion of vacuoles.

The priming step is the only fusion step that is defective when polyphosphate synthesis is absent

Next, we asked which step of the fusion reaction was affected by polyP. Vacuole fusion can be resolved into distinct sub-reactions, such as SNARE activation, trans-SNARE pairing, hemifusion and fusion-pore opening (Ostrowicz et al., 2008; Wickner, 2010). SNARE activation depends on ATP hydrolysis by Sec18/NSF. This chaperone dissociates and activates SNAREs that exist in cis-complexes on vacuoles (Mayer et al., 1996; Ungermann et al., 1998). SNARE activation can be bypassed by adding the purified

Journal of Cell Science (2016) 129, 2817-2828 doi:10.1242/jcs.184382

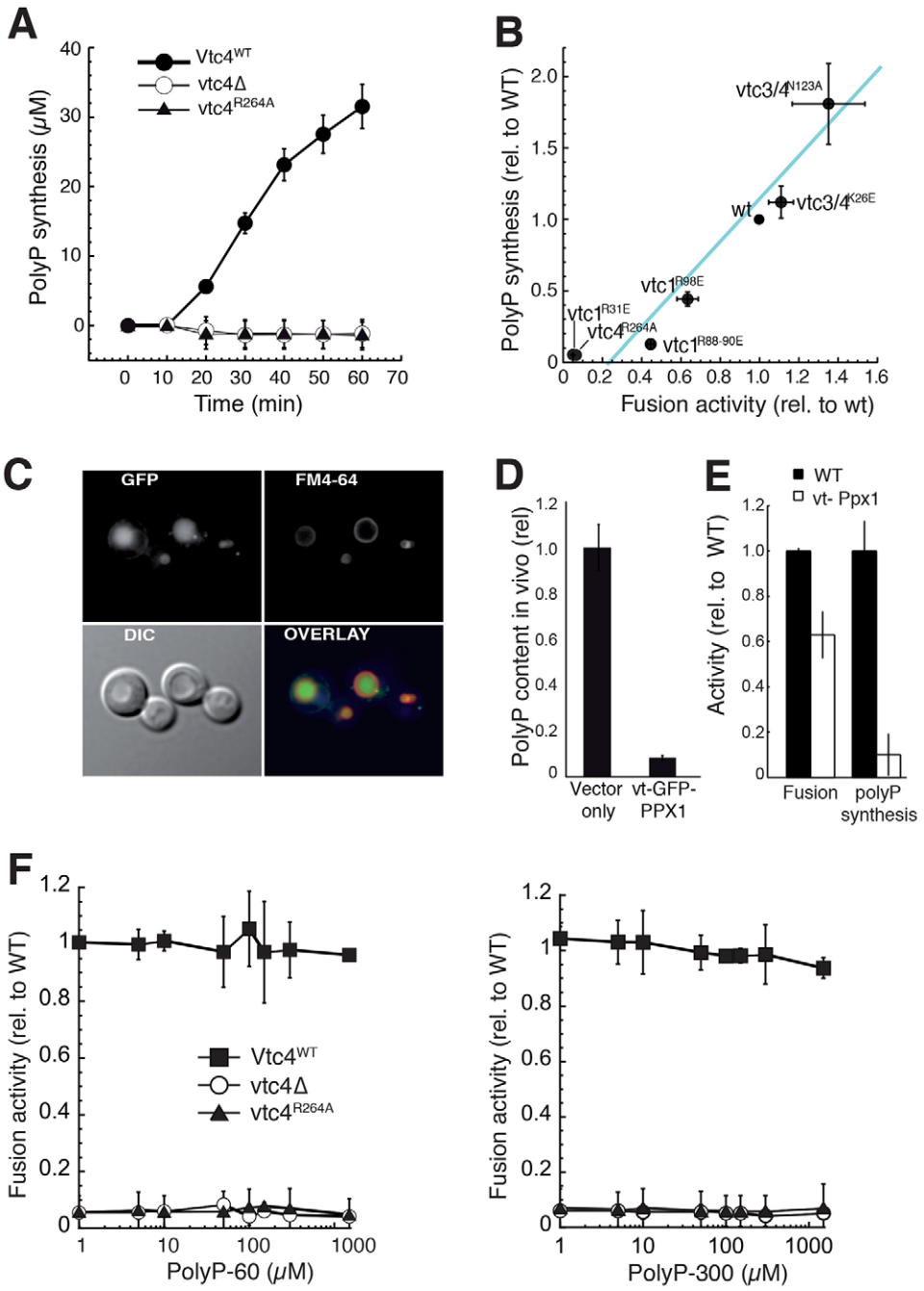

Fig. 2. Influence of vacuolar polyP on vacuole fusion *in vitro*. (A) Vacuoles were purified from BJ3505 *vtc4*Δ cells reconstituted with plasmids expressing wild-type *VTC4* (*Vtc4*^{WT}) or *vtc4*^{R264A}. Isolated organelles were incubated in fusion buffer containing an ATP-regeneration system. At the indicated timepoints, the reaction was stopped by addition of Triton X-100 and EDTA. DAPI was added to quantify newly synthesized polyP. (B) Correlation of fusion activity and polyP synthesis by vacuoles. Vacuoles were isolated from cells expressing either a mutated *vtc1* allele (*vtc1*^{R31E}, *vtc1*^{R98E} and *vtc1*$^{R88-90E}$) or combinations of mutated *vtc3* and *vtc4* alleles (*vtc3*^{K26E}/*vtc4*^{K26E}, *vtc3*^{N120A}/*vtc4*^{N123A}). Fusion activity of these vacuoles was assessed. In parallel, polyP synthesis activity was measured using a fluorescent DAPI-based assay. Values are means of at least three independent experiments and are normalized to values from the wild type. (C) BJ3505 cells carrying the plasmid expressing vacuole-targeted (vt)-Ppx1 (pRS416GPD PPCPY-Ppx1-yeGFP) were grown in HC-URA until an OD_{600nm} of 0.3 was reached. Vacuoles were labeled with FM4-64 as in Fig. 1 and analyzed by fluorescence microscopy. (D) Effect of vt-Ppx1-yeGFP on polyP content *in vivo*. BJ3505 cells had been transformed with the expression plasmid encoding vt-Ppx1-yeGFP or the empty pRS416GPD plasmid only. The cells were grown in HC-URA medium to an OD_{600nm} of 1.0–1.5. PolyP was extracted and quantified using the enzymatic assay (*n*=3). (E) Effect of vt-Ppx1 on polyP accumulation and fusion activity *in vitro*. Fusion activity and polyP accumulation were estimated as in B (*n*=3). (F) Exogenous polyP does not affect vacuole fusion. Vacuoles from the indicated strains were used in fusion reactions in the presence of different concentrations of synthetic polyP of 60 (left) or 300 (right) phosphate units. After 60 min at 27°C, fusion activity was assayed (*n*=3). Concentrations are given in terms of equivalent phosphate units. Data are mean±s.d.

recombinant Q_c-SNARE subunit Vam7, which recruits an existing pool of non-paired, free SNAREs into trans-SNARE complexes and drives fusion in the absence of Sec18/NSF activity (Thorngren et al., 2004). Vam7 addition restored the fusion activity of *vtc4*Δ, *vtc4*^{R264A} and *vtc4*^{K200A} vacuoles to wild-type levels (Fig. 3A). This suggested that trans-SNARE pairing, hemifusion and fusion-pore opening proceed in the absence of polyP and that SNARE activation might be the only step that is affected. We tested SNARE activation directly, using Sec17/α-SNAP, a co-factor of Sec18/NSF. The release of Sec17 from the membrane concurs with the dissociation of cis-SNARE complexes (Mayer et al., 1996; Ungermann et al., 1998). Vacuoles were incubated under fusion conditions and sedimented, and Sec17 was assayed in the membrane pellets and supernatants (Fig. 3B). Release of Sec17 was reduced by 80–95% in vacuoles from *vtc1*Δ, *vtc4*Δ and *vtc4*^{R264A} cells. Vacuoles from *vtc1*^{R98E} cells, which showed an intermediate reduction of polyP synthesis and fusion, showed a reduction in Sec17 release by 30% (Figs 3B and 2B). Also, expression of the vacuole-targeted polyphosphatase Ppx1 reduced Sec17 release by around 30%. Next, we assayed the dissociation of cis-SNARE complexes by performing co-immunoprecipitation of the R-SNARE Nyv1 and the Q_a-SNARE Vam3 (Ungermann et al., 1998). After 15 min of incubation under fusion conditions, vacuoles were solubilized in detergent, and Nyv1 was immunoprecipitated (Fig. 3C). Vam3 co-precipitated with Nyv1 if the preceding incubation of the vacuoles had been performed in the absence of ATP, which leaves Sec18/NSF inactive. Upon incubation in the presence of ATP, the efficiency of co-immunoprecipitation dropped significantly in wild-type vacuoles, but not in *vtc4*^{R264A} or *vtc4*Δ vacuoles (Fig. 3C). This suggests that the ATP-dependent

Journal of Cell Science (2016) 129, 2817-2828 doi:10.1242/jcs.184382

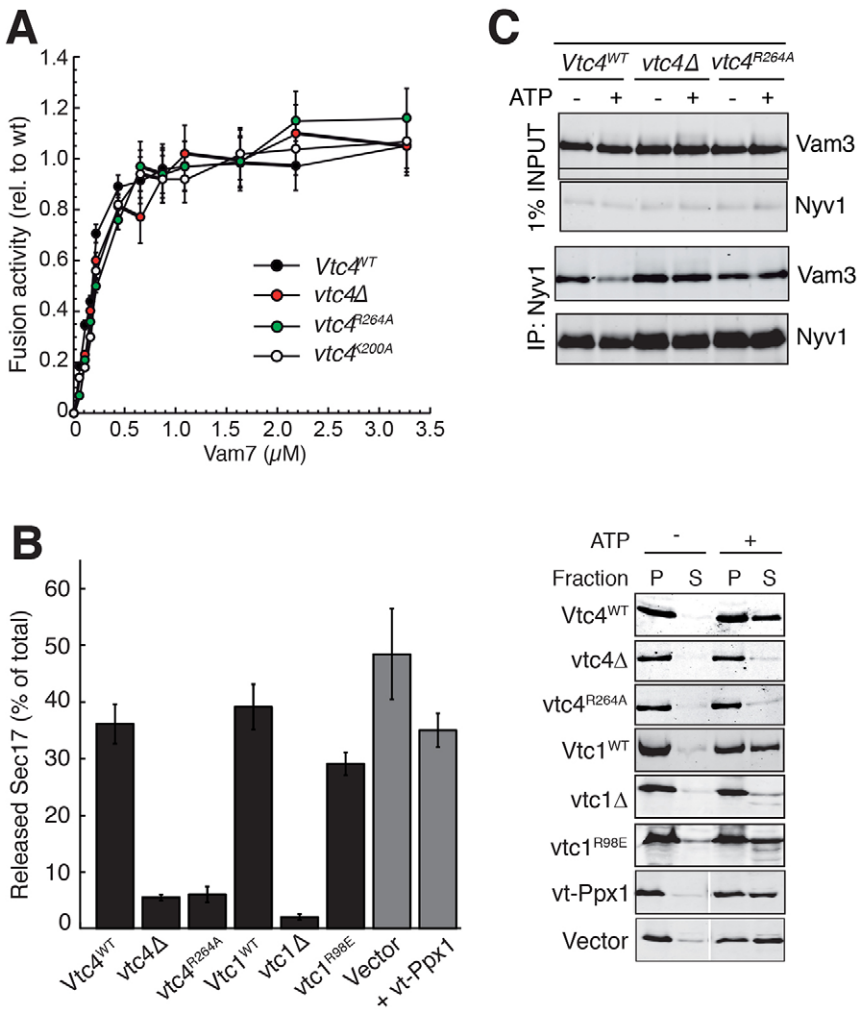

Fig. 3. Effect of polyP on the different steps of vacuole fusion. (A) Bypassing of SNARE activation with recombinant Vam7. Vacuoles from wild-type ($Vtc4^{WT}$), $vtc4\Delta$, $vtc4^{R264A}$ or $vtc4^{K200A}$ cells were incubated in fusion reactions (without ATP-regenerating system) with increasing amounts of recombinant Vam7. After 60 min, fusion was assayed (n=3), and values were normalized to the value from wild type in a normal (with ATP-regenerating system and without Vam7) fusion reaction. (B) Sec17 release. Vacuoles were incubated in fusion reactions with or without ATP at 27°C for 20 min. Vacuoles were sedimented, and Sec17 in the pellets (P) and supernatants (S) was determined by SDS-PAGE and western blotting. Quantification from three independent experiments is shown in the left panel. (C) cis-SNARE separation. Fusion reactions were set up as in B. After 20 min, vacuoles were solubilized and Nyv1 was immunoprecipitated (IP). Co-precipitated proteins were analyzed by SDS-PAGE and western blotting. Data are mean±s.d.

disruption of SNARE complexes depends on the synthesis of polyP and its translocation into the vacuole lumen.

Sec18 is recruited to SNARE complexes only when polyphosphate synthesis occurs

Vacuoles from mutants deficient in polyP synthesis carry normal amounts of Sec18/NSF (Fig. 4A). Therefore, we tested whether their deficiency in SNARE activation might be due to altered interaction of Sec18/NSF with the SNARE complex. Vacuoles were isolated from cells that expressed the SNARE Vam3 with a C-terminal HA tag (Pieren et al., 2010). The membranes were treated with the cleavable crosslinker DTSSP, solubilized in detergent, and immunoprecipitated with anti-HA antibodies. In wild-type vacuoles, Vam3–HA was associated with Sec18/NSF, as expected (Ostrowicz et al., 2008). This association was only detected upon crosslinking. On $vtc4^{R264A}$ and $vtc4\Delta$ vacuoles, Vam3–HA did not interact with Sec18/NSF, whereas it did associate with Nyv1, Vam7 and Sec17, as on wild-type vacuoles (Fig. 4A). This suggests that polyphosphate accumulation facilitates SNARE activation by promoting the interaction of Sec18/NSF with the vacuolar SNARE complex. Therefore, we tested whether fusion between polyP-deficient vacuoles could be activated by excess Sec18/NSF. Overexpressing *SEC18* in a *vtc1*Δ mutant by a factor of >10 over the wild-type level (Fig. 4B–D) rescued the fragmented vacuole phenotype of the *vtc1*Δ mutant and restored 1–2 large vacuoles per cell. Also, the *in vitro* fusion of vacuoles that had been isolated from $vtc4^{R264A}$, $vtc4^{K200A}$ and *vtc4*Δ cells could be restored by incubating them with purified recombinant Sec18/NSF at concentrations that exceeded the endogenous levels by 50 times (Fig. 4E,F).

The vacuolar SNARE Nyv1 and the cyclin Pho80 functionally interact with the VTC complex

The VTC complex physically interacts with Nyv1 (Müller et al., 2003) and genetically interacts with Pho80 (Huang et al., 2002), the cyclin associating with the kinase Pho85. We tested whether these proteins are implicated in the effect of polyphosphates on priming. In absence of Nyv1, the SNAREs remaining on *nyv1*Δ vacuoles – Vam3, Vam7 and Vti1 – must still be activated by Sec18/NSF and Sec17 (Mayer and Wickner, 1997; Nichols et al., 1997; Ungermann et al., 1998). Therefore, SNARE activation can be assayed in *nyv1*Δ vacuoles in the same manner as in wild-type vacuoles. Vacuoles from a *nyv1*Δ *vtc1*Δ double mutant (ΔΔ) showed a significant rescue of Sec17 release to ~70% of that of the wild-type level (Fig. 5A,B). In testing whether deletion of *NYV1* might rescue fusion activity of a *vtc1*Δ vacuoles, we had to consider that vacuole fusion requires Nyv1 on at least one of the fusion partners (Nichols et al., 1997), and we therefore compared the fusion of *vtc1*Δ and ΔΔ vacuoles with wild-type organelles. Although a *vtc1*Δ×wild type combination showed only 40–50% of the fusion signal of a wild type×wild type combination, fusion was rescued to 80–90% in a ΔΔ×wild type combination (Fig. 5C).

Journal of Cell Science (2016) 129, 2817-2828 doi:10.1242/jcs.184382

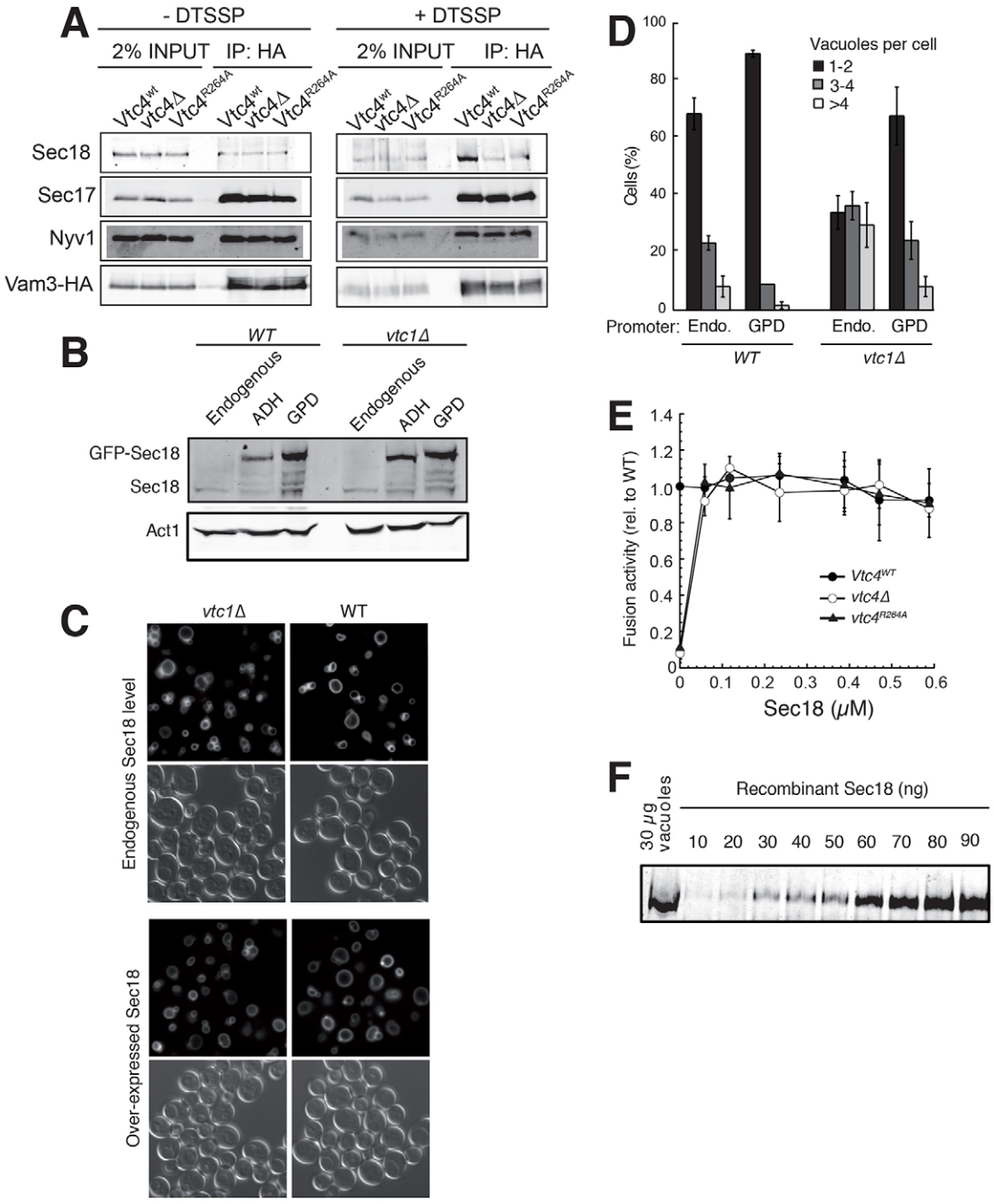

Fig. 4. Sec18 recruitment to SNARE complexes. (A) Interaction with SNAREs. Vacuoles carrying Vam3–HA were incubated with 2 mM DTSSP or with buffer only, and were subjected to immunoprecipitation (IP) with antibodies against HA. Co-immunoprecipitated proteins were reduced in sample buffer with 100 mM DTT (30 min, 50°C) and subjected to SDS-PAGE and western blotting. Comparable results were obtained in three independent experiments. (B) SEC18 overexpression. An ADH or GPD promoter was genomically inserted in front of the SEC18 open reading frame. Wild-type (BY4741) and *vtc1*Δ cells expressing endogenous Sec18 or overexpressing GFP–Sec18 were grown in Hartwell's complete medium to an OD_{600nm} of 1. Total proteins were extracted and subjected to gel electrophoresis and western blotting against Sec18. Actin (Act1) was used as a loading control. Comparable results were obtained in three independent experiments. (C) Vacuole morphology of cells expressing Sec18 from the GPD promoter was assessed as in Fig. 1, and (D) vacuole number per cell was determined (250 cells, *n*=3). Endo, endogenous promoter. (E) *In vitro* fusion with excess Sec18. Vacuoles from the indicated strains were incubated in fusion reactions in the presence of increasing amounts of recombinant Sec18. After 60 min, fusion was assayed. Values are means of three independent experiments and are normalized to values from wild type. (F) Endogenous Sec18 levels on vacuoles. Vacuoles were isolated from BJ3505 cells. 30 µg of protein from the isolated organelles was subjected to gel electrophoresis and western blotting, together with increasing amounts of recombinant Sec18 purified from E.coli. Vacuoles carry around 3 ng of Sec18 per microgram of vacuolar protein. Data are mean±s.d. WT, wild type.

No fusion was observed between two ΔΔ or two *vtc1*Δ vacuoles. This suggests that Nyv1 is necessary for impairing the interaction of Sec18 with the SNAREs in the absence of polyP.

We tested available mutants that were null for Pho85 cyclin genes in a lipid mixing assay to test for *in vitro* vacuole fusion (Reese et al., 2005). Among eight cyclin mutants tested, only vacuoles from

Journal of Cell Science (2016) 129, 2817-2828 doi:10.1242/jcs.184382

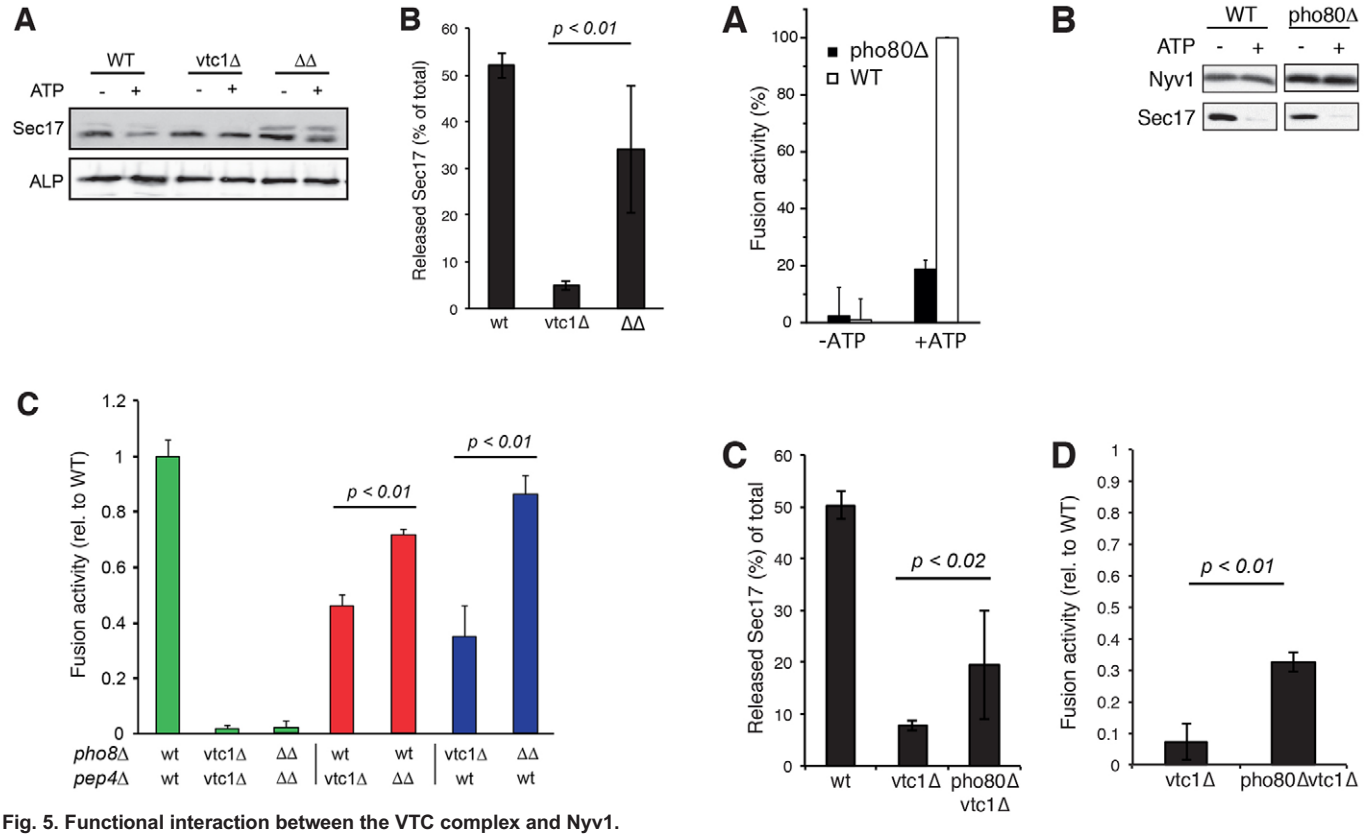

Fig. 5. Functional interaction between the VTC complex and Nyv1. (A) Sec17 release by vacuoles isolated from wild-type (WT, BJ3505) cells or isogenic *vtc1*Δ or *vtc1*Δ *nyv1*Δ (ΔΔ) mutants. The membrane-bound fraction of Sec17 after addition of the ATP-regenerating system or buffer only was estimated by western blotting. Alkaline phosphatase (ALP) was used as a loading control. The amount of released Sec17 was quantified from three different experiments (B). (C) Rescue of fusion in a ΔΔ mutant. Vacuoles were isolated from BJ3505 (*pep4*Δ) and DKY6281 (*pho8*Δ) cells that that carried the ΔΔ or *vtc1*Δ mutations or not. Fusion reactions between these vacuole populations were set up in the indicated combinations and measured using the content mixing assay (*n*=3). Statistical significance was assessed using an unpaired Student's *t*-test. Data are mean±s.d.

*pho80*Δ strains were deficient in lipid mixing (Fig. S3). In content mixing assays, *pho80*Δ vacuoles showed 20% of the activity of wild-type vacuoles (Fig. 6A). *pho80*Δ vacuoles showed normal Sec17 release (Fig. 6B) and SNARE complex disruption (not shown), suggesting that Pho80 was not required for SNARE activation. It might, however, negatively regulate SNARE activation. In this case, a *pho80*Δ *vtc1*Δ double knockout might remedy the defects of *vtc1*Δ vacuoles. Vacuoles from *pho80*Δ *vtc1*Δ cells indeed showed a partial rescue of Sec17 release and of fusion to 30–40% of the wild-type level (Fig. 6C,D). *In vivo*, a *pho80*Δ *vtc1*Δ mutant showed less fragmented vacuoles than *vtc1*Δ cells (Fig. 6E). These data support the hypothesis that polyP accumulation inside vacuoles leads to Pho80–Pho85-dependent changes in the cytosol that influence SNARE activation.

We investigated whether the block of priming was due to a stable modification of the SNARE complex by immuno-adsorbing Vam3–HA-tagged SNARE complexes to protein G-agarose beads. The adsorbed complexes could not be dissociated by simple addition of an ATP regenerating system, suggesting that Sec18/NSF activity had been lost during purification (Fig. 7A). We added back pure Sec18/NSF in increasing concentrations in order to test whether SNARE complexes from *vtc1*Δ and wild-type cells

Fig. 6. Functional interaction between the VTC complex and Pho80. (A) Fusion activity of vacuoles from *pho80*Δ mutants. Vacuoles were isolated from BJ3505 and DKY6281 cells or the derived *pho80*Δ mutants, incubated in the presence or absence of ATP, and fusion was measured by content mixing (*n*=3). Values have been corrected for a 2.1-fold higher abundance of the reporter protein Pho8 in *pho80*Δ vacuoles, which stems from transcriptional activation of *PHO8* in the *pho80*Δ background. (B) Sec17 release from *pho80*Δ vacuoles was assayed under conditions described in A. Nyv1 was used as a loading control. (C) Sec17 release was assayed using vacuoles isolated from strains in which *VTC1* or *PHO80*, or both, had been deleted. The amount of released Sec17 was quantified for three independent experiments. (D) Fusion activity of *vtc1*Δ*pho80*Δ and *vtc1*Δ vacuoles was determined (*n*=3). Values were corrected for a small difference in expression of Pho8, which was 0.92±0.09 U (mean±s.d.) in *vtc1*Δ and 0.82±0.18 U in *vtc1*Δ*pho80*Δ (*n*=3). (E) Vacuole morphology of BY4741, *vtc1*Δ, *pho80*Δ and *pho80*Δ*vtc1*Δ strains was assessed as described in Fig. 1B. Data are mean±s.d.

were equally sensitive to activation by this protein. SNARE activation, measured by release of Sec17 and Vam7 from the beads, showed the same concentration dependence for wild-type and *vtc1*Δ complexes, suggesting that *vtc1*Δ complexes had not retained a stable modification that hindered Sec18/NSF from

Journal of Cell Science (2016) 129, 2817-2828 doi:10.1242/jcs.184382

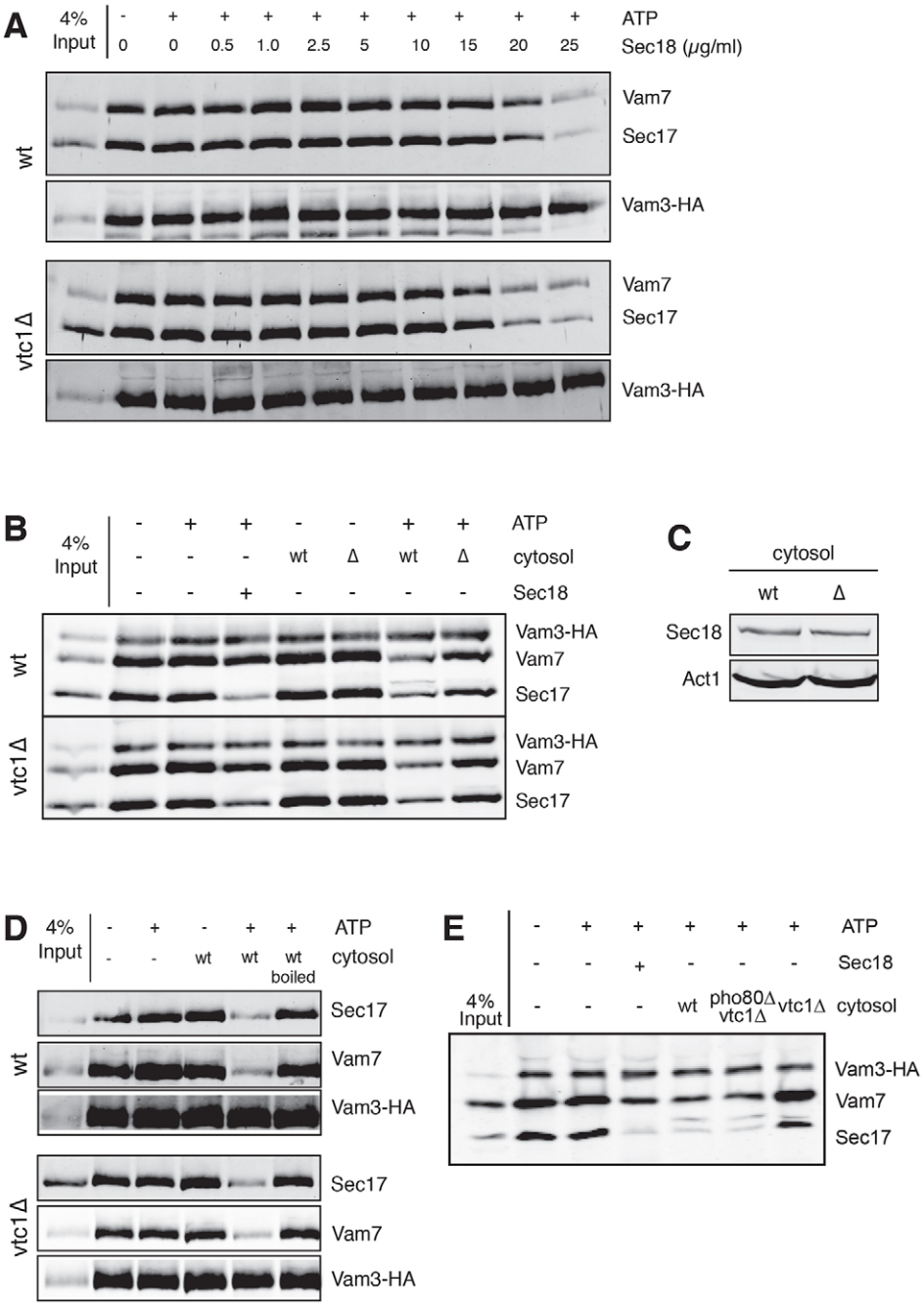

Fig. 7. Dissociation of isolated cis-SNARE complexes by Sec18 and cytosolic extracts from *vtc1*Δ cells. (A) Effect of *vtc* mutant cytosol on vacuoles from wild-type (wt) and *vtc1*Δ cells. Vacuoles were isolated from a BJ3505 and a BJ3505 *vtc1*Δ strain expressing Vam3–HA as the only source of this SNARE. Vacuoles were solubilized in Triton X-100; cis-SNARE complexes were isolated by immunoadsorption and washed with fusion buffer without ATP. The beads were then incubated in the presence or absence of ATP, Sec18 (30 µg/ml) or cytosol (13 mg/ml) from wild-type or *vtc1*Δ cells, as indicated. Proteins pelleted with the beads were analyzed by SDS-PAGE and western blotting. (B) Sensitivity to Sec18. cis-SNARE complexes from wild-type and *vtc1*Δ (Δ) vacuoles were incubated in the presence of increasing concentrations of recombinant Sec18 and ATP, and analyzed for SNARE complex disruption as described in A. (C) Levels of Sec18 in wild-type and *vtc1*Δ cytosol. Samples corresponding to 15 µg of total cytosolic proteins were analyzed by SDS-PAGE and immunoblotting. (D) Effect of heat-inactivated cytosol. The same experiment as described in A was performed, using wild-type cytosol that had been left untreated or had been heat-inactivated at 95°C for 5 min. (E) Effect of cytosol from *vtc1*Δ and *vtc1*Δ *pho80*Δ on SNARE complexes from *vtc1*Δ cells. The same experiment as described in A was performed, using cytosols prepared from the indicated cells or purified recombinant Sec18. Data are mean±s.d.

acting on them. SNARE complex disruption could also be induced by adding wild-type cytosol and ATP, irrespective of whether the vacuoles came from *vtc1*Δ or wild-type cells (Fig. 7B,D). Cytosol from *vtc1*Δ cells was inactive, although it contained the same amount of Sec18 as wild-type cytosol (Fig. 7B,C). By contrast, cytosol from *pho80*Δ *vtc1*Δ cells supported SNARE complex disruption (Fig. 7E), which corroborates the partial rescue of vacuole fusion on *pho80*Δ *vtc1*Δ vacuoles described above. Heating (5 min at 95°C) abolished the activity of cytosol (Fig. 7D), suggesting that the activating effect was not due to the presence of heat-stable low-molecular-mass compounds. Taken together, these data support the hypothesis that cytosolic factors regulate SNARE activation as a function of polyP accumulation in vacuoles, and they implicate Pho80–Pho85 kinase and Nyv1 in this regulation.

DISCUSSION

Vacuole fusion increases the volume of the vacuolar system in response to starvation, accumulation of storage compounds such as polyP, or upon hypotonic shock. The ways in which this volume increase is triggered differ, however. Upon starvation, vacuolar hydrolases are massively upregulated, vacuoles fuse and the volume of the organelle expands, probably in order to accommodate the need for increased degradation through autophagy. In this case, the adjustment occurs over hours rather than minutes and operates through TORC1 kinase. TORC1 is necessary for vacuolar fission but not for vacuole fusion (Michaillat et al., 2012). Because TORC1 activity is downregulated by starvation, starvation tilts the fusion–fission equilibrium towards fusion, leading to a slow net fusion of vacuoles. Interestingly, mammalian lysosomes fuse and undergo a similar increase in volume upon induction of autophagy (Sardiello

Journal of Cell Science (2016) 129, 2817-2828 doi:10.1242/jcs.184382

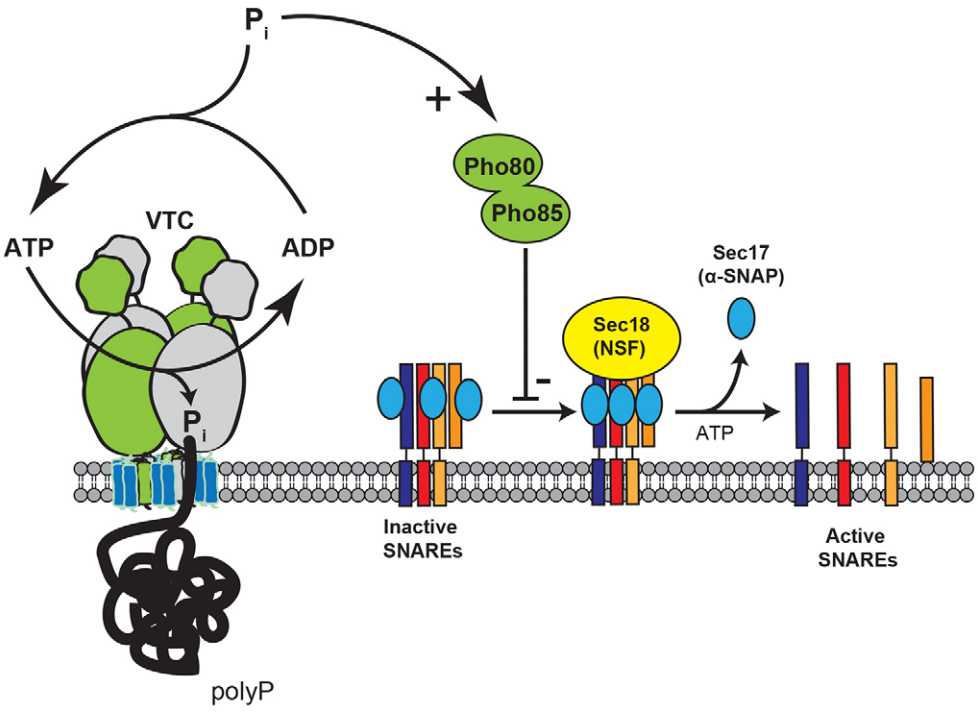

Fig. 8. Working model of the regulation of SNAREs by polyP in the vacuolar lumen. Lumenal polyP signals back into the cytosol in order to promote the activation of SNAREs and vacuole fusion, which in turn increases vacuolar storage space for polyP. We speculate that polyP synthesis, which essentially pumps phosphate from the cytosol into vacuoles, might decrease cytosolic P_i levels. This downregulates Pho80–Pho85 kinase, which negatively regulates binding of Sec18 to vacuolar SNARE complexes. This regulation involves the interaction of VTC with the R-SNARE Nyv1. Data are mean±s.d.

et al., 2009; Yu et al., 2010). In contrast to this slow adaptation to starvation, hypotonic shock increases vacuolar membrane tension very rapidly. Vacuoles fuse in the range of seconds to minutes, probably in order to avoid their lysis. This rapid fusion is induced by a stimulation of the machinery for Rab-GTPase-dependent vacuole docking (Brett and Merz, 2008). The activation of SNAREs is unaffected by membrane tension that is induced by hypotonicity (Brett and Merz, 2008). We have now found that the accumulation of a major vacuolar storage compound stimulates fusion through SNARE activation, controlling the interaction of Sec18/NSF with cis-SNARE complexes. Thus, the vacuolar surface-to-volume ratio can be adjusted through the fusion–fission equilibrium using at least three different molecular pathways. *A priori*, these regulatory inputs are not mutually exclusive. However, polyP-induced fusion of vacuoles is unlikely to depend on osmotic water influx into the lumen of the organelle because polyP chains synthesized by vacuoles are dozens to hundreds of phosphate residues long. The increase of vacuolar osmolarity by such macromolecules should be negligible. PolyP, which is a highly charged polyanion, could also increase the osmotic value of vacuoles by driving an influx of compensatory cations, such as lysine or arginine. Although these amino acids accumulate inside vacuoles up to molar concentrations, they do not lead to a corresponding increase in osmotic pressure, probably because their sequestration by polyP renders them osmotically inert (Dürr et al., 1979). A further argument against the activation of fusion through an osmotic effect of polyP accumulation is that polyP specifically affects SNARE activation and NSF/Sec18 binding, whereas an osmotic increase of membrane tension does not affect this reaction (Brett and Merz, 2008). It is also unlikely that polyP promotes vacuole fusion through TORC1 because vacuole fusion does not require TORC1 activity (Michaillat et al., 2012). Thus, the stimulation of NSF-dependent SNARE activation through the synthesis and lumenal accumulation of polyP represents a previously unidentified regulatory pathway for vacuole size and number that is distinct from the inputs of starvation and osmotic stress.

The fusion defect of *vtc*Δ vacuoles had initially been ascribed to a physical interaction of VTC with the vacuolar H^+-ATPase (Müller et al., 2002, 2003), which is required for vacuole fusion (Bayer et al., 2003; Peters et al., 2001; Sreelatha et al., 2014; Strasser et al., 2011). A function of VTC as the vacuolar polyP polymerase had been dismissed owing to the fact that the complex is entirely oriented towards the cytosol, whereas polyP is located inside the vacuoles. Progress in our understanding of VTC structure and polyP metabolism (Gerasimaite et al., 2014; Hothorn et al., 2009) has now led to the revelation that the crucial factor is indeed vacuolar polyP. This is supported by the effects of point mutants in the catalytic center as well as by artificial expression of a polyphosphatase in the vacuole lumen. Our observations support a model in which polyP accumulation controls fusion through the interaction of Sec18/NSF with the SNARE complex (Fig. 8). We must then postulate that information about the accumulation of polyP inside the organelle is transmitted to the cytosolic face of the membrane where Sec18/NSF and SNAREs interact. An argument in favor of this notion stems from the observation that a cytosolic extract from a wild-type strain promotes SNARE dissociation, an extract from a *vtc1*Δ strain does not and that an extract from a *vtc1*Δ *pho80*Δ mutant restores SNARE activation. This suggests that a crucial factor related to the accumulation of polyP in vacuoles is present in the soluble fraction. How then is the information transmitted? The VTC complex interacts physically with Nyv1 and genetically with Pho80–Pho85 kinase (Huang et al., 2002; Müller et al., 2003). Our data implicate both proteins in the control of SNARE activation because deletion of either of the genes encoding Nyv1 or Pho80 partially rescued the priming defect of *vtc*Δ vacuoles.

The role of Pho80 could be rationalized in the context of its function in the Pho80–Pho85 kinase, which is activated by cytosolic phosphate (Schneider et al., 1994). Because polyP synthesis transfers large amounts of phosphate into vacuoles, thereby lowering cytosolic phosphate concentration (Thomas and O'Shea, 2005), polyP accumulation in vacuoles could be indirectly reported

through the cytosolic phosphate levels (Fig. 8). The lowered cytosolic concentration of phosphate that results from polyP synthesis would reduce Pho80–Pho85 activity, whereas both parameters are expected to increase when polyP synthesis is shut down. Deletion of Pho80 eliminates Pho80–Pho85 kinase activity and would thus mimic a state where polyP is synthesized, promoting SNARE activation. Our attempts to identify relevant Pho80–Pho85-dependent phosphorylation sites have been frustrated by the complexity of the phosphorylation patterns. On the VTC complex alone, we found >20 phosphorylation sites that are strongly up- or downregulated in *pho80*Δ vacuoles relative to wild-type organelles (A.M., unpublished data). Furthermore, we have detected that phosphorylation of residue Ser197 of Nyv1 is upregulated in *vtc4*Δ vacuoles. However, replacing this residue with Ala or Asp did not change vacuolar morphology, fusion activity or the block of priming in *vtc*Δ mutants. A challenge for future analyses will be to take a comprehensive approach that addresses the regulation of the vacuolar fusion machinery by phosphorylation.

MATERIALS AND METHODS

Materials

The following chemicals were bought from the indicated sources: creatine phosphate, creatine kinase, adenosine-5′-triphosphate and protein G-agarose (Roche); dithiothreitol, amino acids, uracil and adenine (AppliChem). 3,3′-dithiobis[sulfosuccinimidylpropionate] (DTSSP) (Pierce). Rhodamine-phosphatidylethanolamine (Rh–PE) and N-(3-triethylammoniumpropyl)-4-(p-diethylaminophenylhexatrienyl)-pyridinium dibromide (FM4-64) (Invitrogen); 4′,6′- diamidino-2-phenylindole (DAPI) (Sigma-Aldrich). Monoclonal anti-hemagglutinin (anti-HA) antibodies (mouse ascites, Covance); poly-peptone and yeast extract (Pronadisa); dextrose and yeast nitrogen base without amino acids and ammonium sulfate (Difco). Polyclonal antibodies against Nyv1, Vam3, Sec17, Sec18, Vtc1 and Vtc4 were raised in rabbits or goats and were prepared as described previously (Müller et al., 2002; Pieren et al., 2010). The lytic enzyme (lyticase), recombinant Sec18, recombinant Ppx1 and recombinant Vam7 were expressed and purified as described previously (Gerasimaite et al., 2014; Müller et al., 2002; Stroupe et al., 2006).

Strains and plasmids

Strains, primers and plasmids used in this study are listed in Tables S1, S2 and S3, respectively. Their generation is described in the appropriate supplementary tables.

Growth medium

Unless indicated otherwise, yeast cells were grown in YPD medium [2% poly-peptone, 1% yeast extract and 2% dextrose (Difco)]. Hartwell's complete medium contained 0.67% yeast nitrogen base without amino acids and ammonium sulfate, 2% dextrose, 0.002% methionine, 0.006% tyrosine, 0.008% isoleucine, 0.005% phenylalanine, 0.01% glutamic acid, 0.02% threonine, 0.01% aspartic acid, 0.015% valine, 0.04% serine, 0.002% arginine, 0.0035% uracil, 0.002% adenine, 0.012% lysine, 0.008% tryptophan, 0.008% leucine and 0.002% histidine.

Vacuole isolation

Vacuoles were isolated as described previously (Pieren et al., 2010). Briefly, yeast were grown overnight in YPD at 30°C. Cells were harvested (1 min, 4000 ***g***, room temperature, JLA-10.500 rotor) at $OD_{600\,nm}$=1.0–1.5, resuspended in 50 ml of 30 mM Tris-HCl pH 8.9 containing 10 mM DTT. After a 5-min incubation at 30°C, cells were sedimented and resuspended in 15 ml of spheroplasting buffer (50 mM potassium phosphate pH 7.5, 600 mM sorbitol in YPD with 0.2% D-glucose and 3600 U ml^{-1} of lyticase). Spheroplasts were obtained after incubation for 26 min at 30°C and sedimented by centrifugation (1 min, 3500 ***g***, 4°C, JA-25.50 rotor). The pellet was gently resuspended in 2.5 ml of 15% Ficoll 400 in PS buffer (10 mM PIPES-KOH pH 6.8, 200 mM sorbitol). Tubes were kept on ice for 2 min before addition of 80 µg or 100 µg DEAE dextran for BJ3505 and DKY6281 or BY4742 strains, respectively. Tubes were transferred to a water bath at 30°C for 90 s and chilled on ice. Spheroplasts were transferred to a SW41 tube and overlaid with 3 ml of 8% Ficoll, 3 ml of 4% Ficoll, and 2 ml 0% Ficoll. After centrifugation (90 min, 150,000 ***g***, 2°C) organelles were collected from the 4%-Ficoll–0%-Ficoll interface. Protein concentrations were determined using a Bradford assay using bovine serum albumin as a standard.

In vitro vacuole fusion

To assay content mixing *in vitro*, 3 µg of vacuoles from BJ3505 and DKY6281 strains were mixed in 30 µl of fusion buffer (PS buffer containing 150 mM KCl and 0.5 mM $MnCl_2$). After addition of an ATP regeneration system (0.5 mM ATP, 0.5 mM $MgCl_2$, 20 mM creatine phosphate, 0.125 mg ml^{-1} creatine kinase, final concentrations), fusion reactions were incubated at 27°C for 60 min. Then, 470 µl of the phosphatase assay mix (10 mM p-nitrophenyl-phosphate, 10 mM $MgCl_2$, 0.4% Triton X-100 in 250 mM Tris-HCl pH 8.9) was added to each tube, and the incubation was prolonged for 5 min at the same temperature. The reaction was stopped by the addition of 500 µl of 1 M glycine-KOH pH 11.5. Absorbance at 400 nm was read with a Spectramax photometer. Values were corrected for a background value obtained with a sample that had been kept on ice during the fusion reaction.

Reporter protein expression of unprocessed Pho8 (pro-Pho8) was assayed by stimulating its activity with Zn^{2+}. 10 mM $ZnCl_2$ was added to 3 µg of vacuoles in 30 µl PS buffer, supplemented with phosphatase assay mix, and alkaline phosphatase activity was developed as described above (Strasser et al., 2011). One unit is equal to the formation of 1 µmole of p-nitrophenol per min and per µg of BJ3505 vacuoles.

Lipid mixing was measured as described previously (Reese et al., 2005). Vacuoles from BY4742 or *vtc* mutants were isolated in the presence of 1× protease inhibitor cocktail (PIC) (7.5 µM pefablock SC, 17.6 nM leupeptin, 3.75 µM o-phenanthroline, 54.7 nM pepstatin A) and 1 mM PMSF. An aliquot of the suspension (186 µg of protein) was diluted to a final volume of 800 µl of PS buffer and equilibrated at 32°C for 40 s. Sixty microliters of Rhodamine–phosphatidylethanolamine (from a 3 mM stock in DMSO) was added drop-wise under continuous slow vortexing. The sample was incubated at 27°C for 2 min. Labeled vacuoles were re-isolated by centrifugation on a discontinuous Ficoll gradient. Mixtures of vacuoles were prepared at a ratio of 1:5 (labeled:unlabeled) in fusion buffer. Fusion reactions were performed in non-coated black 96-well plates that had been pre-incubated with 5% milk in water. Reactions were started by adding an ATP-regeneration system to the samples. Fluorescence changes (λ_{exc}=540 nm, λ_{em}=590 nm) were recorded with a SpectraMax Gemini XS plate reader at 27°C. Measurements were taken every 2 min for 32 min. At the end, 0.5% Triton X-100 (final concentration) was added to the sample, and fluorescence intensities were recorded for 10 min.

PolyP assays

PolyP synthesis was followed using DAPI (Gerasimaite et al., 2014). 5 µg of vacuoles were suspended in a total volume of 100 µl at a concentration of 0.05 mg ml^{-1} in fusion buffer containing an ATP-regeneration system (1 mM ATP, 1 mM $MgCl_2$, 40 mM creatine phosphate and 0.25 mg ml^{-1} creatine kinase). Samples were incubated at 27°C for the indicated time. The reaction was stopped by the addition of Stop Solution (8 mM EDTA, 0.1% Triton X-100 and 10 µM DAPI, final concentrations). 250 µl was transferred to a black 96-well plate, and fluorescence intensity (λ_{exc}=415 nm, λ_{em}=550 nm) was measured with a SpectraMax GEMINI XS fluorescence plate reader.

Polyphosphate accumulation in whole cells was measured as described previously (Hothorn et al., 2009), except that the cells were grown in Hartwell's complete medium or in Hartwell's complete medium lacking uracil until an OD_{600nm} of around 1.5 was reached. Then, 1 OD unit of cells was harvested by centrifugation (14,000 ***g***, 1 min, 20°C), resuspended in 50 µl of 1 M sulfuric acid, and vortexed for 10 s. An equal volume of 2 M sodium hydroxide was added to restore a neutral pH, and samples were vortexed again for 10 s. Two volumes of 1 M Tris-malate buffer pH 7.4 were added before the samples were briefly vortexed. Polyphosphate was purified on DNA-binding columns (Qiagen PCR purification Kit). The washing

buffer was 10 mM Tris-HCl pH 7.0 containing 50% ethanol, 10 mM NaCl and 0.3 mM EDTA. The final elution was performed in 110 µl of the commercial Elution Buffer. 50 µl of the extracts was mixed in a white 96-well plate with an equal volume of 2× polyphosphatase buffer (10 mM Tris-HCl pH 7.0, 3 mM $MgCl_2$) containing 0.01 µg $µl^{-1}$ of the recombinant exopolyphosphatase Ppx1, or buffer only. Samples were incubated at 37°C for 1.5 h before addition of 150 µl of the malachite green reagent (86 µl of 28 mM ammonium heptamolybdate in 2.1 M sulfuric acid and 64 µl of 0.76 mM malachite green in 0.35% polyvinyl alcohol). Absorption at 595 nm was measured using a microplate photometer.

Sec17 release

Vacuoles were suspended in 60 µl of fusion buffer at a concentration of 0.24 mg ml^{-1}. ATP-regeneration system or buffer was added to the reaction mixtures before the tubes were placed at 27°C for 15 min. Samples were then put back on ice and diluted to 400 µl with fusion buffer and immediately centrifuged (20,000 ***g***, 20 min, 4°C). Pellets were washed once with fusion buffer and transferred to a new tube. Proteins in the supernatant were trichloroacetic-acid-precipitated (12.5% final concentration). Samples were then resuspended in loading buffer and analyzed by SDS-PAGE and western blotting. Signals were detected by using a LICOR Odyssey infrared fluorescence scanner and quantified with its software.

cis-SNARE disruption assay

For cis-SNARE disruption assays, 90 µg of vacuoles were diluted in fusion buffer to a concentration of 0.2 mg ml^{-1}. Then, ATP-regeneration system or buffer was added as described for the content mixing assay, and samples were incubated for 20 min at 27°C. Vacuoles were harvested by centrifugation (7 min, 7000 ***g***, 4°C) and resuspended in lysis buffer (20 mM HEPES buffer pH 7.4, 150 mM KCl, 0.5% Triton X-100, 10% glycerol, 1 mM PMSF, 1× PIC). Samples were solubilized by gentle agitation for 20 min at 4°C, and insoluble material was removed by centrifugation (15 min, 20,000 ***g***, 4°C). Proteins in the supernatant were immunoprecipitated using immunoprecipitated using 1.5 µl of mouse ascites (Covance) containing anti-HA antibodies or 2 µg of affinity-purified anti-Nyv1 antibodies and 20 µl of protein-G agarose beads. After a 45-min incubation period at 4°C, beads were washed three times with a washing buffer (20 mM HEPES pH 7.4, 150 mM KCl, 0.2% Triton X- 100, 10% glycerol, 1 mM PMSF, 1× PIC). Proteins were eluted by heating the beads at 95°C for 5 min in 2× loading buffer for SDS-PAGE.

For cis-SNARE disruption assays on beads, vacuoles were solubilized in the lysis buffer, and insoluble materials were removed by centrifugation (15 min, 20,000 ***g***, 4°C). Protein-G agarose beads and anti-HA antibodies were added to the supernatant, and immunoprecipitation was performed as described above. Beads were then washed three times with lysis buffer. $MnCl_2$ was then added to a final concentration of 0.5 mM. Samples were then incubated at 27°C for 20 min with additives where indicated. Beads were recovered by centrifugation and washed three times with the washing buffer. Samples were then processed as described above. When needed, cytosols were boiled (5 min at 95°C), and insoluble material was removed by centrifugation (15 min, 20,000 ***g***, 4°C). The supernatant was used as 'boiled cytosol'.

Reversible crosslinking followed by immunoprecipitation

Proteins on isolated vacuoles were first crosslinked with the cleavable amine-reactive crosslinker DTSSP [3,3′-dithiobis (sulfosuccinimidylpropionate)]. 200 µg of isolated vacuoles was pelleted by centrifugation (7000 ***g***, 10 min, 4°C) and resuspended in 700 µl of 20 mM HEPES buffer pH 7.4 containing 200 mM sorbitol 150 mM KCl and 2 mM DTSSP. Samples were incubated at 4°C with end-over-end agitation for 60 min. The reaction was quenched by the addition of 20 mM Tris-HCl pH 7.5, 150 mM KCl, 200 mM sorbitol (final concentrations), and the incubation was continued at 30°C for 30 min. Vacuoles were isolated by centrifugation (10,000 ***g***, 10 min, 4°C), resuspended in lysis buffer, and immunoprecipitation was performed as described above. Samples were reduced in SDS- PAGE loading buffer containing 100 mM DTT for 30 min at 50°C.

Microscopy

Vacuole morphology was determined by FM4-64 staining of the vacuole membrane. Cells were grown overnight in Hartwell's complete medium to an OD_{600nm} of 0.4–1.0. Cultures were diluted to an OD_{600nm} of 0.3, and FM4-64 was added at a final concentration of 10 µM. Cells were incubated for 1.5 h at 25°C, washed in medium without dye and finally resuspended in fresh medium. The cells were further incubated at 25°C for 2 h, concentrated in their medium by short and mild centrifugation, resuspended in one-tenth of the supernatant and then analyzed with microscopy. For the localization of GFP-tagged proteins, cells were grown in Hartwell's complete medium lacking uracil (HC-URA) to logarithmic phase. Vacuoles were labeled as previously described, and the cells were analyzed with fluorescence microscopy. Microscopy was done on a LEICA DMI6000B inverted microscope equipped with a Hamamatsu digital CCD camera (ORCA-R2 C10600-10B), an X-Cite® series 120Q UV lamp and a Leica 100×1.4 NA lens. Pictures were collected with Perkin Elmer Volocity software and analyzed with the open-source software ImageJ.

Statistics

Unless stated otherwise, data points with error bars represent the mean of three independent experiments. Error bars represent the standard deviation.

Acknowledgements

We thank Andrea Schmidt and Véronique Comte for assistance and the members of our laboratory for discussion.

Competing interests

The authors declare no competing or financial interests.

Author contributions

Y.D. and H.N. conceived, performed and interpreted the experiments and wrote the manuscript. A.M. conceived and interpreted experiments and wrote the manuscript.

Funding

This work was supported by grants from the Swiss National Science Foundation (Schweizerischer Nationalfonds zur Förderung der Wissenschaftlichen Forschung) [grant numbers 144258 and 163477/1]; and the European Research Council to A.M. [grant number 233458].

Supplementary information

Supplementary information available online at
http://jcs.biologists.org/lookup/doi/10.1242/jcs.184382.supplemental

References

Baars, T. L., Petri, S., Peters, C. and Mayer, A. (2007). Role of the V-ATPase in regulation of the vacuolar fission-fusion equilibrium. *Mol. Biol. Cell* **18**, 3873-3882.

Banta, L. M., Robinson, J. S., Klionsky, D. J. and Emr, S. D. (1988). Organelle assembly in yeast: characterization of yeast mutants defective in vacuolar biogenesis and protein sorting. *J. Cell Biol.* **107**, 1369-1383.

Bayer, M. J., Reese, C., Bühler, S., Peters, C. and Mayer, A. (2003). Vacuole membrane fusion: V0 functions after trans-SNARE pairing and is coupled to the Ca2+-releasing channel. *J. Cell Biol.* **162**, 211-222.

Bevis, B. J., Hammond, A. T., Reinke, C. A. and Glick, B. S. (2002). De novo formation of transitional ER sites and Golgi structures in Pichia pastoris. *Nat. Cell Biol.* **4**, 750-756.

Bhave, M., Papanikou, E., Iyer, P., Pandya, K., Jain, B. K., Ganguly, A., Sharma, C., Pawar, K., Austin, J., Day, K. J. et al. (2014). Golgi enlargement in Arf-depleted yeast cells is due to altered dynamics of cisternal maturation. *J. Cell Sci.* **127**, 250-257.

Brett, C. L. and Merz, A. J. (2008). Osmotic regulation of Rab-mediated organelle docking. *Curr. Biol.* **18**, 1072-1077.

Chan, Y.-H. M. and Marshall, W. F. (2012). How cells know the size of their organelles. *Science* **337**, 1186-1189.

Chan, Y.-H. M. and Marshall, W. F. (2014). Organelle size scaling of the budding yeast vacuole is tuned by membrane trafficking rates. *Biophys. J.* **106**, 1986-1996.

Derganc, J., Antonny, B. and Copič, A. (2013). Membrane bending: the power of protein imbalance. *Trends Biochem. Sci.* **38**, 576-584.

Dove, S. K., Piper, R. C., McEwen, R. K., Yu, J. W., King, M. C., Hughes, D. C., Thuring, J., Holmes, A. B., Cooke, F. T., Michell, R. H. et al. (2004). Svp1p defines a family of phosphatidylinositol 3,5-bisphosphate effectors. *EMBO J.* **23**, 1922-1933.

Dürr, M., Urech, K., Boller, T., Wiemken, A., Schwencke, J. and Nagy, M. (1979). Sequestration of arginine by polyphosphate in vacuoles of yeast (Saccharomyces cerevisiae). *Arch. Microbiol.* **121**, 169-175.
Efe, J. A., Botelho, R. J. and Emr, S. D. (2007). Atg18 regulates organelle morphology and Fab1 kinase activity independent of its membrane recruitment by phosphatidylinositol 3,5-bisphosphate. *Mol. Biol. Cell* **18**, 4232-4244.
Ellis, R. J. (2001). Macromolecular crowding: an important but neglected aspect of the intracellular environment. *Curr. Opin. Struct. Biol.* **11**, 114-119.
Frolov, V. A., Shnyrova, A. V. and Zimmerberg, J. (2011). Lipid polymorphisms and membrane shape. *Cold Spring Harb. Perspect. Biol.* **3**, a004747.
García-Pérez, A. I., López-Beltrán, E. A., Klüner, P., Luque, J., Ballesteros, P. and Cerdán, S. (1999). Molecular crowding and viscosity as determinants of translational diffusion of metabolites in subcellular organelles. *Arch. Biochem. Biophys.* **362**, 329-338.
Gaynor, E. C., Chen, C. Y., Emr, S. D. and Graham, T. R. (1998). ARF is required for maintenance of yeast Golgi and endosome structure and function. *Mol. Biol. Cell* **9**, 653-670.
Gerasimaite, R., Sharma, S., Desfougères, Y., Schmidt, A. and Mayer, A. (2014). Coupled synthesis and translocation restrains polyphosphate to acidocalcisome-like vacuoles and prevents its toxicity. *J. Cell Sci.* **127**, 5093-5104.
Hamill, O. P. and Martinac, B. (2001). Molecular basis of mechanotransduction in living cells. *Physiol. Rev.* **81**, 685-740.
Heald, R. and Cohen-Fix, O. (2014). Morphology and function of membrane-bound organelles. *Curr. Opin. Cell Biol.* **26**, 79-86.
Hothorn, M., Neumann, H., Lenherr, E. D., Wehner, M., Rybin, V., Hassa, P. O., Uttenweiler, A., Reinhardt, M., Schmidt, A., Seiler, J. et al. (2009). Catalytic core of a membrane-associated eukaryotic polyphosphate polymerase. *Science* **324**, 513-516.
Huang, D., Moffat, J. and Andrews, B. (2002). Dissection of a complex phenotype by functional genomics reveals roles for the yeast cyclin-dependent protein kinase Pho85 in stress adaptation and cell integrity. *Mol. Cell. Biol.* **22**, 5076-5088.
Hürlimann, H. C., Stadler-Waibel, M., Werner, T. P. and Freimoser, F. M. (2007). Pho91 is a vacuolar phosphate transporter that regulates phosphate and polyphosphate metabolism in Saccharomyces cerevisiae. *Mol. Biol. Cell* **18**, 4438-4445.
Katsura, I. (1987). Determination of bacteriophage λ tail length by a protein ruler. *Nature* **327**, 73-75.
Kitamoto, K., Yoshizawa, K., Ohsumi, Y. and Anraku, Y. (1988). Dynamic aspects of vacuolar and cytosolic amino acid pools of Saccharomyces cerevisiae. *J. Bacteriol.* **170**, 2683-2686.
Levy, D. L. and Heald, R. (2010). Nuclear size is regulated by importin α and Ntf2 in Xenopus. *Cell* **143**, 288-298.
Lonetti, A., Szijgyarto, Z., Bosh, D., Loss, O., Azevedo, C. and Saiardi, A. (2011). Identification of an evolutionary conserved family of inorganic polyphosphate endopolyphosphatases. *J. Biol. Chem.* **286**, 31966-31974.
Ludington, W. B., Shi, L. Z., Zhu, Q., Berns, M. W. and Marshall, W. F. (2012). Organelle size equalization by a constitutive process. *Curr. Biol.* **22**, 2173-2179.
Marshall, W. F. (2012). Organelle size control systems: from cell geometry to organelle-directed medicine. *BioEssays* **34**, 721-724.
Mayer, A. and Wickner, W. (1997). Docking of yeast vacuoles is catalyzed by the Ras-like GTPase Ypt7p after symmetric priming by Sec18p (NSF). *J. Cell Biol.* **136**, 307-317.
Mayer, A., Wickner, W. and Haas, A. (1996). Sec18p (NSF)-driven release of Sec17p (alpha-SNAP) can precede docking and fusion of yeast vacuoles. *Cell* **85**, 83-94.
Michaillat, L., Baars, T. L. and Mayer, A. (2012). Cell-free reconstitution of vacuole membrane fragmentation reveals regulation of vacuole size and number by TORC1. *Mol. Biol. Cell* **23**, 881-895.
Müller, O., Johnson, D. I. and Mayer, A. (2001). Cdc42p functions at the docking stage of yeast vacuole membrane fusion. *EMBO J.* **20**, 5657-5665.
Müller, O., Bayer, M. J., Peters, C., Andersen, J. S., Mann, M. and Mayer, A. (2002). The Vtc proteins in vacuole fusion: coupling NSF activity to V(0) trans-complex formation. *EMBO J.* **21**, 259-269.
Müller, O., Neumann, H., Bayer, M. J. and Mayer, A. (2003). Role of the Vtc proteins in V-ATPase stability and membrane trafficking. *J. Cell Sci.* **116**, 1107-1115.
Nichols, B. J., Ungermann, C., Pelham, H. R. B., Wickner, W. T. and Haas, A. (1997). Homotypic vacuolar fusion mediated by t- and v-SNAREs. *Nature* **387**, 199-202.
Omelon, S., Georgiou, J. and Habraken, W. (2016). A cautionary (spectral) tail: red-shifted fluorescence by DAPI-DAPI interactions. *Biochem. Soc. Trans.* **44**, 46-49.
Ostrowicz, C. W., Meiringer, C. T. A. and Ungermann, C. (2008). Yeast vacuole fusion: a model system for eukaryotic endomembrane dynamics. *Autophagy* **4**, 5-19.
Peters, C., Bayer, M. J., Bühler, S., Andersen, J. S., Mann, M. and Mayer, A. (2001). Trans-complex formation by proteolipid channels in the terminal phase of membrane fusion. *Nature* **409**, 581-588.
Peters, C., Baars, T. L., Buhler, S. and Mayer, A. (2004). Mutual control of membrane fission and fusion proteins. *Cell* **119**, 667-678.
Pieren, M., Schmidt, A. and Mayer, A. (2010). The SM protein Vps33 and the t-SNARE H(abc) domain promote fusion pore opening. *Nat. Struct. Mol. Biol.* **17**, 710-717.
Pisoni, R. L. and Lindley, E. R. (1992). Incorporation of [32P]orthophosphate into long chains of inorganic polyphosphate within lysosomes of human fibroblasts. *J. Biol. Chem.* **267**, 3626-3631.
Rafelski, S. M. and Marshall, W. F. (2008). Building the cell: design principles of cellular architecture. *Nat. Rev. Mol. Cell Biol.* **9**, 593-602.
Reese, C., Heise, F. and Mayer, A. (2005). Trans-SNARE pairing can precede a hemifusion intermediate in intracellular membrane fusion. *Nature* **436**, 410-414.
Saito, K., Ohtomo, R., Kuga-Uetake, Y., Aono, T. and Saito, M. (2005). Direct labeling of polyphosphate at the ultrastructural level in Saccharomyces cerevisiae by using the affinity of the polyphosphate binding domain of Escherichia coli exopolyphosphatase. *Appl. Environ. Microbiol.* **71**, 5692-5701.
Sardiello, M., Palmieri, M., di Ronza, A., Medina, D. L., Valenza, M., Gennarino, V. A., Di Malta, C., Donaudy, F., Embrione, V., Polishchuk, R. S. et al. (2009). A gene network regulating lysosomal biogenesis and function. *Science* **325**, 473-477.
Schneider, K. R., Smith, R. L. and O'Shea, E. K. (1994). Phosphate-regulated inactivation of the kinase PHO80-PHO85 by the CDK inhibitor PHO81. *Science* **266**, 122-126.
Seeley, E. S., Kato, M., Margolis, N., Wickner, W. and Eitzen, G. (2002). Genomic analysis of homotypic vacuole fusion. **13**, 782-794.
Settembre, C., Zoncu, R., Medina, D. L., Vetrini, F., Erdin, S., Erdin, S., Huynh, T., Ferron, M., Karsenty, G., Vellard, M. C. et al. (2012). A lysosome-to-nucleus signalling mechanism senses and regulates the lysosome via mTOR and TFEB. *EMBO J.* **31**, 1095-1108.
Sreelatha, A., Bennett, T. L., Carpinone, E. M., O'Brien, K. M., Jordan, K. D., Burdette, D. L., Orth, K. and Starai, V. J. (2014). Vibrio effector protein VopQ inhibits fusion of V-ATPase-containing membranes. *Proc. Natl. Acad. Sci. USA* **112**, 100-105.
Strasser, B., Iwaszkiewicz, J., Michielin, O. and Mayer, A. (2011). The V-ATPase proteolipid cylinder promotes the lipid-mixing stage of SNARE-dependent fusion of yeast vacuoles. *EMBO J.* **30**, 4126-4141.
Stroupe, C., Collins, K. M., Fratti, R. A. and Wickner, W. (2006). Purification of active HOPS complex reveals its affinities for phosphoinositides and the SNARE Vam7p. *EMBO J.* **25**, 1579-1589.
Sukharev, S. and Sachs, F. (2012). Molecular force transduction by ion channels: diversity and unifying principles. *J. Cell Sci.* **125**, 3075-3083.
Tamura, N., Oku, M., Ito, M., Noda, N. N., Inagaki, F. and Sakai, Y. (2013). Atg18 phosphoregulation controls organellar dynamics by modulating its phosphoinositide-binding activity. *J. Cell Biol.* **202**, 685-698.
Thomas, M. R. and O'Shea, E. K. (2005). An intracellular phosphate buffer filters transient fluctuations in extracellular phosphate levels. *Proc. Natl. Acad. Sci. USA* **102**, 9565-9570.
Thorngren, N., Collins, K. M., Fratti, R. A., Wickner, W. and Merz, A. J. (2004). A soluble SNARE drives rapid docking, bypassing ATP and Sec17/18p for vacuole fusion. *EMBO J.* **23**, 2765-2776.
Ungermann, C., Nichols, B. J., Pelham, H. R. B. and Wickner, W. (1998). A vacuolar v-t-SNARE complex, the predominant form in vivo and on isolated vacuoles, is disassembled and activated for docking and fusion. *J. Cell Biol.* **140**, 61-69.
Upadhyaya, A. and Sheetz, M. P. (2004). Tension in tubulovesicular networks of Golgi and endoplasmic reticulum membranes. *Biophys. J.* **86**, 2923-2928.
Vida, T. A. and Emr, S. D. (1995). A new vital stain for visualizing vacuolar membrane dynamics and endocytosis in yeast. *J. Cell Biol.* **128**, 779-792.
Weisman, L. S. (2003). Yeast Vacuole Inheritance and Dynamics. *Annu. Rev. Genet* **37**, 435-460.
Wickner, W. (2010). Membrane fusion: five lipids, four SNAREs, three chaperones, two nucleotides, and a Rab, all dancing in a ring on yeast vacuoles. *Annu. Rev. Cell Dev. Biol.* **26**, 115-136.
Wild, R., Gerasimaite, R., Jung, J.-Y., Truffault, V., Pavlovic, I. Schmidt, A., Saiardi, A., Jessen, H. J., Poirier, Y., Hothorn, M. and Mayer, A. (2016). Control of eukaryotic phosphate homeostasis by inositol polyphosphate sensor domains. *Science* **352**, 986-990.
Wurst, H. and Kornberg, A. (1994). A soluble exopolyphosphatase of Saccharomyces cerevisiae. Purification and characterization. *J. Biol. Chem.* **269**, 10996-11001.
Yu, L., McPhee, C. K., Zheng, L., Mardones, G. A., Rong, Y., Peng, J., Mi, N., Zhao, Y., Liu, Z., Wan, F. et al. (2010). Termination of autophagy and reformation of lysosomes regulated by mTOR. *Nature* **465**, 942-946.
Zhou, H.-X., Rivas, G. and Minton, A. P. (2008). Macromolecular crowding and confinement: biochemical, biophysical, and potential physiological consequences. *Annu. Rev. Biophys.* **37**, 375-397.
Zieger, M. and Mayer, A. (2012). Yeast vacuoles fragment in an asymmetrical two-phase process with distinct protein requirements. **23**, 3438-3449.

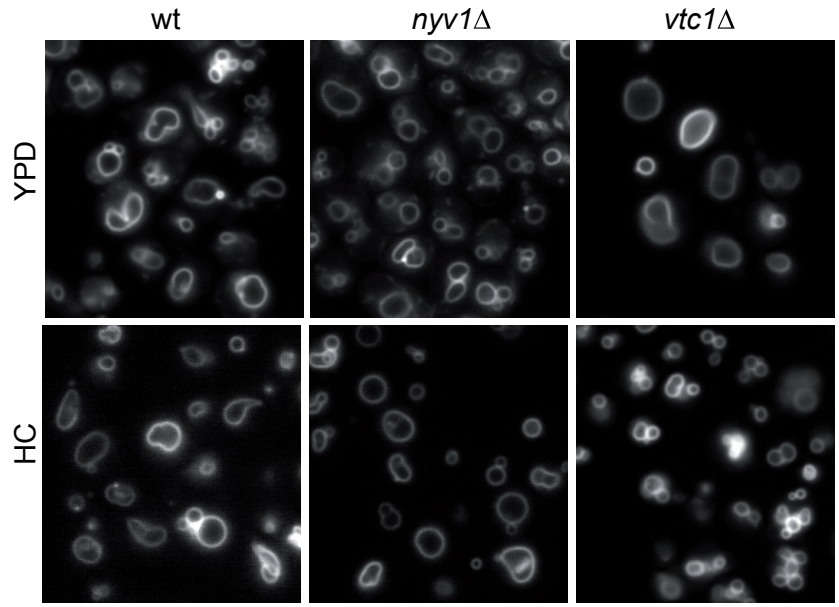

Fig. S1

The indicated strains were grown to logarithmic phase in YPD or HC medium, stained with FM4-64 and analyzed by fluorescence microscopy. Culture on HC favors transition of vtc1δ vacuoles to a more fragmented state, but does not change structure of nyv1δ vacuoles.

Fig. S2

vt-GFP-PPX1 remains intact in protease-deficient BJ3505 cells.
BJ3505 cells expressing the construct were grown logarithmically in YPD. After sedimentation, whole cell protein extracts were prepared and analyzed by SDS-PAGE and Western blotting against GFP.

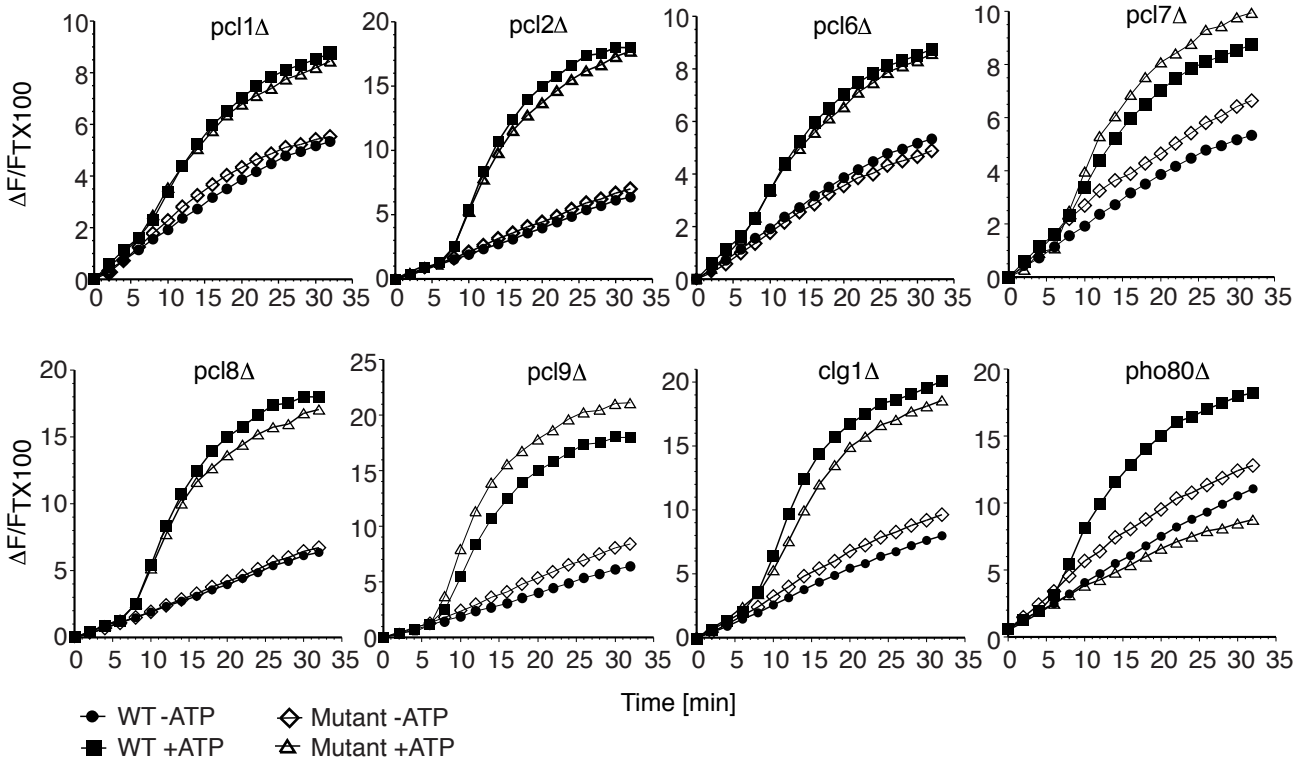

Fig. S3

Fusion activity of vacuoles from pho85Δ cyclin null mutants.
Vacuoles were isolated from BY4742 or the indicated derived mutants and fusion was measured using the lipid mixing assay. Similar results have been obtained in three independent experiments.

Table S1. Strains used in this study.

Deletion strains were obtained by replacing the complete ORF of a given gene with the KanMX or natNT2 resistance cassettes amplified from plasmids pUG6 or pFA6-clonnath, respectively (Euroscarf). VTC1 was replaced by the kanMX marker using primers 1 and 2. VTC1 was replaced by the natNT2 marker using primers 3 and 4. VTC4 was deleted using primers 5 and 6. Deletion of the genes was verified by Western blotting. PHO80 was deleted using primers 7 and 8. For the introduction of the GPD promoter in front of the SEC18 ORF, the GPD promoter fused to yeGFP was amplified from the plasmid pYM-N17 using primers 9 and 10. Correct integration was verified by colony PCR using primers 11 and 12, and Western blotting. Yeast transformations were performed using the lithium acetate procedure as describe before.

Name	Genotype	Reference
BJ3505	Mata pep4::HIS3 prb1-Δ1.6R lys2-208 trp1-Δ101 ura3-52 gal2 can	(Jones et al., 1982)
DKY6281	MATα PHO8::TRP1 LEU2-3 LEU2-112 lys2-801 suc2-Δ9 trp1-Δ901 ura3-52	(Haas et al., 1994)
BY4741	MATa his3Δ1 leu2Δ0 met15Δ0 ura3Δ0	Euroscarf
BY4742	MATα his3Δ1 leu2Δ0 lys2Δ0 ura3Δ0	Euroscarf
BY4742 vtc4Δ	MATα his3Δ1 leu2Δ0 lys2Δ0 ura3Δ0 vtc4::kanMX	Euroscarf
BY4741 vtc1Δ	MATa his3Δ1 leu2Δ0 met15Δ0 ura3Δ0 vtc1::kanMX	Euroscarf
BY4742 $vtc4^{wt}$	MATα his3Δ1 leu2Δ0 lys2Δ0 ura3Δ0 vtc4::kanMX + pRS303 $vtc4^{wt}$	(Hothorn et al., 2009)
BY4742 $vtc4^{R264A}$	MATα his3Δ1 leu2Δ0 lys2Δ0 ura3Δ0 vtc4::kanMX + pRS303 $vtc4^{R264A}$	(Hothorn et al., 2009)
BJ3505 vtc4Δ	Mata pep4::HIS3 prb1-Δ1.6R lys2-208 trp1-Δ101 ura3-52 gal2 can vtc4::KanMX	This study
BJ3505 $vtc4^{wt}$	Mata pep4::HIS3 prb1-Δ1.6R lys2-208 trp1-Δ101 ura3-52 gal2 can vtc4::KanMX + pRS306 $Vtc4^{wt}$	This study
BJ3505 $vtc4^{R264A}$	Mata pep4::HIS3 prb1-Δ1.6R lys2-208 trp1-Δ101 ura3-52 gal2 can vtc4::KanMX + pRS306 $Vtc4^{R264A}$	This study
BJ3505 $vtc4^{K200A}$	Mata pep4::HIS3 prb1-Δ1.6R lys2-208 trp1-Δ101 ura3-52 gal2 can vtc4::KanMX + pRS306 $Vtc4^{K200A}$	This study
DKY6281 vtc4Δ	MATα PHO8::TRP1 LEU2-3 LEU2-112 lys2-801 suc2-Δ9 trp1-Δ901 ura3-52 vtc4::natNT2	This study
DKY6281 $vtc4^{wt}$	MATα PHO8::TRP1 LEU2-3 LEU2-112 lys2-801 suc2-Δ9 trp1-Δ901 ura3-52 vtc4::natNT2 + pRS306 $Vtc4^{wt}$	This study
DKY6281 $vtc4^{R264A}$	MATα PHO8::TRP1 LEU2-3 LEU2-112	This study

	lys2-801 suc2-Δ9 trp1-Δ901 ura3-52 vtc4::natNT2 + pRS306 Vtc4^{R264A}	
DKY6281 vtc4^{K200A}	MATα PHO8::TRP1 LEU2-3 LEU2-112 lys2-801 suc2-Δ9 trp1-Δ901 ura3-52 vtc4::natNT2 + pRS306 Vtc4^{K200A}	This study
BJ3505 vtc1Δ	Mata pep4::HIS3 prb1-Δ1.6R lys2-208 trp1-Δ101 ura3-52 gal2 can vtc1::KanMX	This study
BJ3505 vtc1^{wt}	Mata pep4::HIS3 prb1-Δ1.6R lys2-208 trp1-Δ101 ura3-52 gal2 can vtc1::KanMX + pRS304 vtc1^{wt}	This study
BJ3505 vtc1R31E	Mata pep4::HIS3 prb1-Δ1.6R lys2-208 trp1-Δ101 ura3-52 gal2 can vtc1::KanMX + pRS304 vtc1^{R31E}	This study
BJ3505 vtc1R88-90E	Mata pep4::HIS3 prb1-Δ1.6R lys2-208 trp1-Δ101 ura3-52 gal2 can vtc1::KanMX + pRS304 vtc1$^{R88-90E}$	This study
BJ3505 vtc1R98E	Mata pep4::HIS3 prb1-Δ1.6R lys2-208 trp1-Δ101 ura3-52 gal2 can vtc1::KanMX + pRS304 vtc1^{R98E}	This study
DKY6281 vtc1Δ	MATα PHO8::TRP1 LEU2-3 LEU2-112 lys2-801 suc2-Δ9 trp1-Δ901 ura3-52 vtc1::HIS3	(Müller et al., 2002)
DKY6281 vtc1^{wt}	MATα PHO8::TRP1 LEU2-3 LEU2-112 lys2-801 suc2-Δ9 trp1-Δ901 ura3-52 vtc1::HIS3 + pRS306 vtc1^{wt}	This study
DKY6281 vtc1R31E	MATα PHO8::TRP1 LEU2-3 LEU2-112 lys2-801 suc2-Δ9 trp1-Δ901 ura3-52 vtc1::HIS3 + pRS306 vtc1^{R31E}	This study
DKY6281 vtc1R88-90E	MATα PHO8::TRP1 LEU2-3 LEU2-112 lys2-801 suc2-Δ9 trp1-Δ901 ura3-52 vtc1::HIS3 + pRS306 vtc1$^{R88-90E}$	This study
DKY6281 vtc1R98E	MATα PHO8::TRP1 LEU2-3 LEU2-112 lys2-801 suc2-Δ9 trp1-Δ901 ura3-52 vtc1::HIS3 + pRS306 vtc1^{R98E}	This study
BY4742 vtc4Δ vtc3Δ vtc2Δ vtc4^{wt} vtc3^{wt}	MATα his3Δ1 leu2Δ0 lys2Δ0 ura3Δ0 vtc4::kanMX vtc2::LEU2 vtc3::natNT2 + pRS303 VTC4^{wt} + pRS306 VTC3^{wt}	This study
BY4742 vtc4Δ vtc3Δ vtc2Δ vtc4^{N123A} vtc3^{N120A}	MATα his3Δ1 leu2Δ0 lys2Δ0 ura3Δ0 vtc4::kanMX vtc2::LEU2 vtc3::natNT2 + pRS303 VTC4^{N123A} + pRS306 VTC3^{N120A}	This study
BY4742 vtc4Δ vtc3Δ vtc2Δ vtc4^{K26E} vtc3^{K26E}	MATα his3Δ1 leu2Δ0 lys2Δ0 ura3Δ0 vtc4::kanMX vtc2::LEU2 vtc3::natNT2 + pRS303 VTC4^{K26E} + pRS306 VTC3^{K26E}	This study
BJ3505 vt-PPX1	Mata pep4::HIS3 prb1-Δ1.6R lys2-208 trp1-Δ101 ura3-52 gal2 can + pRS416 GPD PPCPY-PPX1	This study
DKY6281 vt-PPX1	MATα PHO8::TRP1 LEU2-3 LEU2-112 lys2-801 suc2-Δ9 trp1-Δ901 ura3-52 + pRS416 GPD PPCPY-PPX1	This study

BJ3505 Vam3-HA vtc4Δ	Mata pep4::HIS3 prb1-Δ1.6R lys2-208 trp1-Δ101 ura3-52 gal2 can vam3(His)$_6$(HA)$_3$ vtc4::natNT2	This study
BJ3505 Vam3-HA vtc4^{wt}	Mata pep4::HIS3 prb1-Δ1.6R lys2-208 trp1-Δ101 ura3-52 gal2 can vtc4::natNT2 + pRS306 vtc4^{wt}	This study
BJ3505 Vam3-HA vtc4^{R264A}	Mata pep4::HIS3 prb1-Δ1.6R lys2-208 trp1-Δ101 ura3-52 gal2 can vtc4::natNT2 + pRS306 vtc4^{R264A}	This study
BY4741 P$_{GPD}$ GFP-Sec18	MATa his3Δ1 leu2Δ0 met15Δ0 ura3Δ0 P$_{GPD}$ GFP-Sec18 (natNT2)	This study
BY4741 vtc1Δ P$_{GPD}$ GFP-Sec18	MATa his3Δ1 leu2Δ0 met15Δ0 ura3Δ0 vtc1::KanMX P$_{GPD}$ GFP-Sec18 (natNT2)	This study
BJ3505 nyv1Δ	Mata pep4::HIS3 prb1-Δ1.6R lys2-208 trp1-Δ101 ura3-52 gal2 can nyv1::TRP1	(Nichols et al. 1997)
BJ3505 nyv1Δ vtc1Δ	Mata pep4::HIS3 prb1-Δ1.6R lys2-208 trp1-Δ101 ura3-52 gal2 can nyv1::TRP1 vtc1::KanMX	This study
BJ3505 pho80Δ vtc1Δ	Mata pep4::HIS3 prb1-Δ1.6R lys2-208 trp1-Δ101 ura3-52 gal2 can pho80::kanMX vtc1::natNT2	This study
DKY6281 pho80Δ vtc1Δ	MATα PHO8::TRP1 LEU2-3 LEU2-112 lys2-801 suc2-Δ9 trp1-Δ901 ura3-52 pho80::kanMX vtc1::natNT2	This study
BY4742 pcl1Δ	MATα his3Δ1 leu2Δ0 lys2Δ0 ura3Δ0 pcl1::kanMX	Euroscarf
BY4742 pcl2Δ	MATα his3Δ1 leu2Δ0 lys2Δ0 ura3Δ0 pcl2::kanMX	Euroscarf
BY4742 pcl6Δ	MATα his3Δ1 leu2Δ0 lys2Δ0 ura3Δ0 pcl6::kanMX	Euroscarf
BY4742 pcl7Δ	MATα his3Δ1 leu2Δ0 lys2Δ0 ura3Δ0 pcl7::kanMX	Euroscarf
BY4742 pcl8Δ	MATα his3Δ1 leu2Δ0 lys2Δ0 ura3Δ0 pcl8::kanMX	Euroscarf
BY4742 pcl9Δ	MATα his3Δ1 leu2Δ0 lys2Δ0 ura3Δ0 pcl9::kanMX	Euroscarf
BY4742 clg1Δ	MATα his3Δ1 leu2Δ0 lys2Δ0 ura3Δ0 clg1::kanMX	Euroscarf
BY4742 pho80Δ	MATα his3Δ1 leu2Δ0 lys2Δ0 ura3Δ0 pho80::kanMX	Euroscarf

Table S2. Primers used in this study

Name	Sequence
Primer 1	CTA CAT TAT CGA ATA CGA TTA AAC ACT ACG CCA GAT TTC CAC AAT ATG CAG CTG AAG CTT CGT ACG C
Primer 2	AGT TTG TGC GTA ACC CAC GCT TAC GAT ATT GGA ATT ACA ATT TCA GCA TAG GCC ACT AGT GGA TCT G
Primer 3	CTA CAT TAT CGA ATA CGA TTA AAC ACT ACG CCA GAT TTC CAC AAT ATG CGT ACG CTG CAG GTC GAC
Primer 4	CAG TTT GTG CGT AAC CCA CGC TTA CGA TAT TGG AAT TAC AAT TTC AAT CGA TGA ATT CGA GCT CG
Primer 5	GGC TAA CAA TCA AAT CGG CCA ATA AAA GAG CAT AAC AAG GCA GGA ACA GCT ATG CGT ACG CTG CAG GTC GAC
Primer 6	GAT TAT TAC TTA ATT ATA CAG TAA AAA AAA CAC GCT GTG TAT TCA TTT AAT CGA TGA ATT CGA GCT CG
Primer 7	ATA AGT GTT TAT CAA ATT TAA GTC TGC AAG CTA TCA TAA GAC GAG GAT CAG CTG AAG CTT CGT ACG C
Primer 8	TCA TTA ATC TGG CTT TGA TCG CTT GTT ATA GAT ATG TGC GTC CGC ATA GGC CAC TAG TGG ATC TG
Primer 9	GAT AAG AGC AAA TAG TAC CGT ATA TTC AGC CTT TAT AAA TTG AGT ATG CGT ACG CTG CAG GTC GAC
Primer 10	TCT GGT GGA GTA TGA TTT GCA GCA GCT TTT CCA AAA CCA GGT ATC TTG AAC ATC GAT GAA TTC TCT GTC G
Primer 11	CGT AGC CTT TAA GTA CTA CCG T
Primer 12	GTC TGC AGC GAG GAG CCG TA

Table S3. Plasmids used in this study

Name	
pRS306 Vtc4^{wt}	insert (promoter VTC4-VTC4 ORF) was cut from pRS303 Vtc4^{wt} (Hothorn et al., 2009), using XhoI and SacI and ligated in pRS306; the resulting plasmid was integrated in the VTC4 locus after linearization with MfeI
pRS306 Vtc4^{R264A}	insert (promoter VTC4-VTC4 ORF) was cut from pRS303 Vtc4^{R264A} (Hothorn et al., 2009), using XhoI and SacI and ligated in pRS306; the resulting plasmid was integrated in the VTC4 locus after linearization with MfeI
pRS306 Vtc4^{K200A}	insert (promoter VTC4-VTC4 ORF) was cut from pRS303 Vtc4^{K200A} (Hothorn et al., 2009), using XhoI and SacI and ligated in pRS306; the resulting plasmid was integrated in the VTC4 locus after linearization with MfeI
pRS306 vtc1^{wt}	insert (promoter VTC1-VTC1 ORF) was cut from pRS304 Vtc1^{wt} (Hothorn et al., 2009), using XhoI and NotI and ligated in pRS306; the resulting plasmid was integrated in the URA3 locus after linearization with StuI
pRS306 vtc1^{R31E}	insert (promoter VTC1-VTC1 ORF) was cut from pRS304 Vtc1^{R31E} (Hothorn et al., 2009), using XhoI and NotI and ligated in pRS306; the resulting plasmid was integrated in the URA3 locus after linearization with StuI
pRS306 vtc1$^{R88-90E}$	insert (promoter VTC1-VTC1 ORF) was cut from pRS304 Vtc1$^{R88-90E}$ (Hothorn et al., 2009), using XhoI and NotI and ligated in pRS306; the resulting plasmid was integrated in the URA3 locus after linearization with StuI
pRS306 vtc1^{R98E}	insert (promoter VTC1-VTC1 ORF) was cut from pRS304 Vtc1^{R98E} (Hothorn et al., 2009), using XhoI and NotI and ligated in pRS306; the resulting plasmid was integrated in the URA3 locus after linearization with StuI
pRS303 VTC4^{wt}	(Hothorn et al., 2009)
pRS303 VTC4^{K26E}	VTC4 was mutagenized using primers: forward 5'- TAG TTA TGA TGA TCT GGA GAC TGA GCT AGA AGA TAA CTT ATC TAA G -3' reverse 5'- CTT CTA G CT CAG TCT CCA GAT CAT CAT AAC TAA TAT AAT AGT AGC TG -3'
pRS303 VTC4^{N123A}	VTC4 was mutagenized using primers: forward 5'- AAA GTT TTC GAG ACT AGC CTA CAC TGG TTT CCA AAA GAT TAT CAA GAA C -3' reverse 5'- TGG AAA CCA GTG TAG GCT AGT CTC GAA AAC TTT GCT AGA TCA TGA ACA TCG -3'
pRS306 VTC3^{wt}	VTC3 (with its own promoter) was amplified from yeast genomic DNA using primers: forward 5'- ACT GAG CTC TTC GGC GGA CTC CAA CTA TTA GAT A -3' reverse 5'- ACT GAA TTC TTC CCC AAC CAA ATT GAA GA

	-3' and ligated into pRS306 after digestion with SacI and EcoRI
pRS306 VTC3^{K26E}	VTC3 was mutagenized using primers: forward 5'- GAC TAT GAA AGG TTG GAG AAA TTA CTA AAG GAA AGC GTC ATA CAT G -3' reverse 5'- CCT TTA GTA ATT TCT CCA ACC TTT CAT AGT CGA TAT ATG AAT CCT TCC -3'
pRS306 VTC3^{N120A}	VTC3 was mutagenized using primers: forward 5'- AAC TTT GAC AGG TTA GCT TTT ACT GGG TTT ATC AAG ATT GTG AAG AAA CAC G -3' reverse 5'- AAC TTT GAC AGG TTA GCT TTT ACT GGG TTT ATC AAG ATT GTG AAG AAA CAC G -3'
pRS416 GPD PPCPY-PPX1	(Gerasimaite et al., 2014)

References

Gerasimaitė R, Sharma S, Desfougères Y, Schmidt A, Mayer A (2014) Coupled synthesis and translocation restrains polyphosphate to acidocalcisome-like vacuoles and prevents its toxicity. *J Cell Sci* **127**: 5093–5104.

Haas, A., B. Conradt, and W. Wickner. 1994. G-protein ligands inhibit in vitro reactions of vacuole inheritance. *J Cell Biol*. 126:87–97.

Hothorn, M., H. Neumann, E.D. Lenherr, M. Wehner, V. Rybin, P.O. Hassa, A. Uttenweiler, M. Reinhardt, A. Schmidt, J. Seiler, A.G. Ladurner, C. Herrmann, K. Scheffzek, and A. Mayer. 2009. Catalytic core of a membrane-associated eukaryotic polyphosphate polymerase. *Science*. 324:513–516. doi:10.1126/science.1168120.

Jones, E.W., G.S. Zubenko, and R.R. Parker. 1982. PEP4 gene function is required for expression of several vacuolar hydrolases in Saccharomyces cerevisiae. *Genetics*. 102:665–677.

Müller, O., M.J. Bayer, C. Peters, J.S. Andersen, M. Mann, and A. Mayer. 2002. The Vtc proteins in vacuole fusion: coupling NSF activity to V(0) trans-complex formation. *EMBO J*. 21:259–269. doi:10.1093/emboj/21.3.259.